OPEN ACCESS
IOP Publishing
Nanotechnology

Nanotechnology **36** (2025) 072001 (24pp) https://doi.org/10.1088/1361-6528/ad958c

Topical Review

Quantum dots synthesis within ternary III–V nanowire towards light emitters in quantum photonic circuits: a review

Giorgos Boras*, Haotian Zeng*, Jae-Seong Park, Huiwen Deng, Mingchu Tang and Huiyun Liu

Department of Electronic and Electrical Engineering, University College London, London WC1 E7J, United Kingdom

E-mail: g.boras@ucl.ac.uk and haotian.zeng.13@ucl.ac.uk

Received 1 April 2024, revised 20 September 2024
Accepted for publication 21 November 2024
Published 29 November 2024

Abstract

The positioning of quantum dots (QDs) in nanowires (NWs) on-axis has emerged as a controllable method of QD fabrication that has given rise to structures with exciting potential in novel applications in the field of Si photonics. In particular, III–V NWQDs attract a great deal of interest owing to their vibrant optical properties, high carrier mobility, facilitation in integration with Si and bandgap tunability, which render them highly versatile. Moreover, unlike Stranski–Krastanov or self-assembled QDs, this configuration allows for deterministic position and size of the dots, enhancing the sample uniformity and enabling beneficial functions. Among these functions, single photon emission has presented significant interest due to its key role in quantum information processing. This has led to efforts for the integration of ternary III–V NWQD non-classical light emitters on-chip, which is promising for the commercial expansion of quantum photonic circuits. In the current review, we will describe the recent progress in the synthesis of ternary III–V NWQDs, including the growth methods and the material platforms in the available literature. Furthermore, we will present the results related to single photon emission and the integration of III–V NWQDs as single photon sources in quantum photonic circuits, highlighting their promising potential in quantum information processing. Our work demonstrates the up-to-date landscape in this field of research and pronounces the importance of ternary III–V NWQDs in quantum information and optoelectronic applications.

Keywords: nanowire quantum dots, ternary, III–V, single photon emission, quantum information

* Authors to whom any correspondence should be addressed.

1. Introduction

The synthesis of III–V nanowires (NWs) has been a topic of extensive research due to their potential for implementation in devices with ultra-low volume, high efficiency and low power consumption [1, 2]. Their morphological uniqueness allows for efficient strain relaxation along their sidewalls, enabling the monolithic integration of lattice-mismatched materials [3]. This has led to important achievements, including the monolithic integration of optically active group III–V semiconductors with the mature Si platform, which is the foundation for most optoelectronic circuits [4].

Moreover, a material platform that extends the versatility of NW structures is ternary III–V alloys, which provide an additional degree of freedom in the design, due to the bandgap modulation via controlling the elemental composition [5]. The successful fabrication of ternary III–V NWs is demanding because of the sensitivity to the growth parameters, including the V/III ratio, temperature, source fluxes and contamination in the chamber. Despite these issues, a variety of III–V ternary NWs have been realized over the past years [6–15]. Some of the most notable examples include GaAsP [6–9], GaAsSb [10–13], and InGaAs [14, 15], which allowed for the investigation of infrared emission and its applicability for telecommunication applications.

On the other hand, another type of nanostructures for wide-scale implementation in Si photonics is quantum dots (QDs). Due to their zero-dimensionality leading to strong quantum confinement, QDs are ideal for use in novel applications such as single photon generation, which is crucial for quantum information processing [16, 17]. One common growth method for QDs is the Stranski–Krastanov (SK) mode. It is a strain-driven procedure, signifying that lattice-mismatched materials can be combined [18]. Despite their success, the random nature of strain renders the control of the position and dimensions of the dot challenging. Hence, another alternative was imperative to deterministically regulate these parameters. One important solution is the embedding of the QDs in NWs by stacking a narrower bandgap material along the NW axis, leading to the formation of nanowire quantum dots (NWQDs). One prominent feature of NWQDs, compared to other types of QDs, is that they are naturally confined in one direction along the NW elongation axis, while further confinement occurs by the barrier material along the NW. This can be accomplished by modulating the elemental supply during growth, thus achieving a precisely controlled dot position and size [19]. Ternary III–V NWQDs in particular present increased interest due to the bandgap tunability, increasing the range of emission that can be achieved [19]. Over the recent years, the acquired structures have been implemented in several applications including single photon sources [20–22] and light-emitting diodes (LEDs) [23], while entangled photon pair generation with potential use in quantum circuits has also been reported [24]. In addition, NWQDs have been successfully implemented in laser fabrication [25–27].

Apart from their suitability for optoelectronic device applications, NWQDs are promising for functionality in novel, emerging quantum technologies, which, albeit immature, have attracted a large amount of scientific research and commercial attention over the past few years. An area of particular focus for NWQD research is quantum information processing, which utilizes the superposition of photons to optically store and transmit data [28]. The elemental unit which is called a 'qubit' is ideally comprised of a single photon. Initially, regardless of the high interest, the intangible nature of the superposition states rendered the subject an academic topic of discussion rather than a pragmatic scientific venture. Nevertheless, the introduction of quantum algorithms in 1994 [29], and their predicted power in terms of data speed and volume increased the practicality of quantum computing. In that regard, QDs are highly promising because their strong carrier confinement enables the generation of single that possess key properties for quantum computing such as high brightness, interconnectivity and indistinguishability [30]. Over the past decade, quantum-controlled NOT gates based on single photons have been realized; a giant step towards quantum information processing [31–33]. Furthermore, multiqubit entanglement gates have been achieved, which is favorable towards scalable quantum computing [34]. Besides, on-chip integration of single photon sources has been a subject of scrutiny and study, with significant advancements having been achieved [35–37]. Hence, the aforementioned progress has rendered the analysis, research and commercialization of quantum computing not only a topic of scientific curiosity but a realistic, potential attainment of the near future. Considering the role of single photons as carriers of quantum information and the suitability of dot-in-wire structures as single photon emitters, the described achievements constitute the study and comprehension of NWQDs and their function imperative.

In this review, we will present the recent progress in the growth and characterization of III–V NWQDs and demonstrate their role in single photon generation. The investigation of the relevant literature allowed us to encapsulate the material platforms, highlight the most important findings and discuss the potential for device fabrication. Initially, we will introduce the growth methods for NWQDs, namely the selective area growth (SAG), vapor–liquid–solid (VLS) growth, and catalyst-free techniques, and mention the peculiarities of each of them. Furthermore, we will explore the various ternary III–V NWQDs realized in the past, subcategorized into two groups: those with GaAs QD as the active region and those with ternary III–V material as the active region. Due to their importance, we will also include works related to III-nitride-based NWQDs, separately. Besides, we will address the vibrant topic of quantum information processing and the prominent role of ternary III–V NWQDs and eventually, we will describe the integration of III–V NWQD single photon sources in quantum photonic circuits, which is promising for the large-scale, commercial application of these nanostructures in quantum computing and quantum networks.

2. Growth techniques

One of the primary points of focus in the design of efficient and functioning nanostructures is the growth technique that

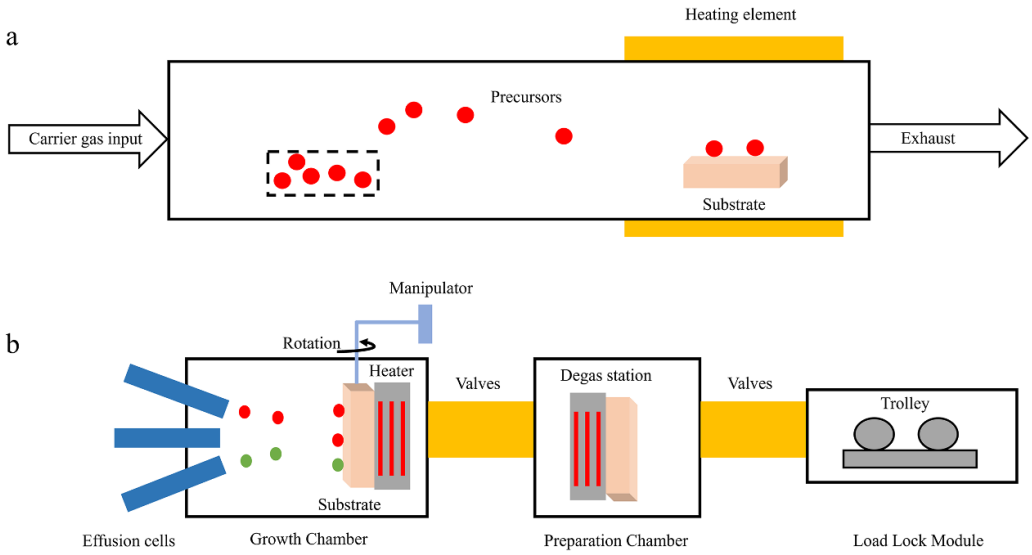

Figure 1. (a) Schematic representation of a typical CVD system, where usually argon or nitrogen are used as carrier gases. (b) Basic schematics of a typical MBE system, where the sample is loaded via the load lock module and is then transferred initially to the preparation chamber for thermal annealing and eventually in the growth chamber, where adatoms are ballistically emitted towards a substrate from effusion cells.

is adopted. The most prevalent method in silicon-based technology for a wide range of material systems including group III–V, group IV semiconductors, nitrides and perovskites is epitaxy. During epitaxial growth, material layers are formed in well-defined orientations, while the initiation of the growth stems from a seed layer. This technique is particularly important for compound semiconductor materials and ternary alloys, as it allows for precise control over the dimensions and position of the deposited layer, while technological advances have enabled the acquisition of crystalline layers with exquisite material quality.

Among the various epitaxial growth systems that have been developed, molecular beam epitaxy (MBE) and metal-organic vapor phase epitaxy (MOVPE), which is also known as metal-organic chemical vapor deposition (MOCVD) are of high significance due to their unique advantages. MOVPE is a material deposition method where the substrate receives elemental precursors that react with each other, forming the material layers. This is highly important in thin film synthesis, with the deposition of precursors occurring via the use of gas argon or nitrogen acting as carrier gas. Hence, the main feature of MOVPE is the material growth based on chemical reactions under intermediate pressure. A schematic representation of a typical MOVPE system is demonstrated in figure 1(a).

Opposite to MOVPE, MBE is a physical evaporation procedure that was invented in the 1960s [38], where adatoms are transferred as beam flux on the surface of a substrate wafer. The procedure is conducted under ultra-high vacuum (UHV), signifying that no chemical interaction takes place among the adatoms prior to their arrival on the substrate. Interestingly, due to the UHV conditions, the deposition of atoms occurs ballistically, ensuring high control over the material growth, while the slow growth rate allows for high material quality and purity without dopants or contaminants. Figure 1(b) includes a schematic representation of a typical MBE system, which is comprised of three chambers, the load-lock, the buffer chamber and the growth chamber. The load-lock is the only part of the reactor that comes in contact with atmospheric air and is used to load and unload samples and wafers in the MBE system via a trolley. The buffer chamber is used to store wafers or samples and is also a space where the substrates are annealed, mounted to a heater at the degas station for decontamination prior to their introduction to the growth chamber. Finally, the latter is the heart of the MBE system, where the material synthesis occurs via the aforementioned technique. The substrate is positioned facing the effusion cells, which are heated so that solid elements begin to sublime. The precursors reach the substrate ballistically. The substrate is heated via a heating station and can be rotated via a manipulator in order for the material deposition to be uniform. It is interesting to mention that valves are used between the different MBE system components to avoid contamination.

It is interesting to highlight that in the case of NWQDs that are described in the current review, the two major growth approaches are the top-down and the bottom-up approach. During the former, the 1D structures are etched down from bulk materials, after they are coated with a hard mask [39]. This is followed by the extensive use of lithography, most commonly electron beam lithography (EBL) and dry or wet etching. Sacrificial etching that can be adopted is a powerful tool that is considered compatible with thin film fabrication techniques which are widely popular in industrial applications. Nevertheless, the most important challenge associated with the top-down NW fabrication is the quality of the obtained materials. The additional processing steps, most importantly etching, lead to rougher surfaces, while, as the fabrication is conducted

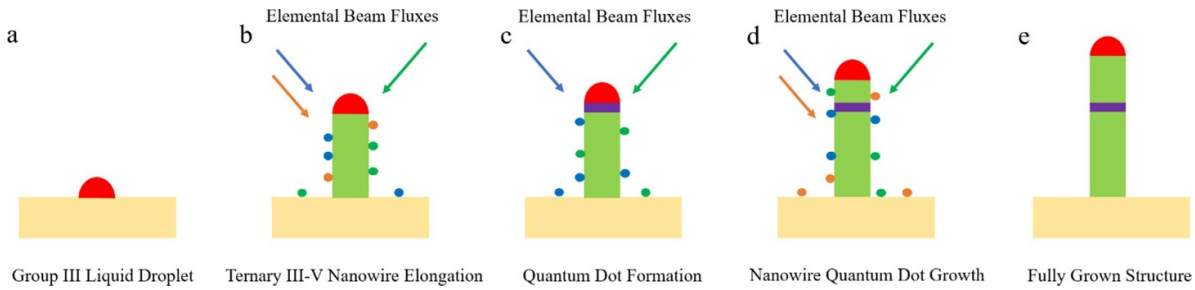

Figure 2. (a) The group III liquid droplet is deposited on the substrate. (b) The III–V elemental fluxes are introduced, and the NW starts to grow. (c) The supply of one element is terminated, which leads to the QD segment formation. (d) The supply of the element is restored, which causes the development of the top NW part. (e) The NWQD is fully grown.

in already-grown bulk materials, the acquired NWs present a high density of crystal defects, including threading dislocations that are degrading to the optical response of the structures. Due to these challenges, the reports on top-down fabrication of III–V NWQDs are limited and only describe binary, GaAs/InAs NWQDs [40–42].

The most popular approach for NWs and NWQDs, including III–V and nitrides is bottom-up. The structural synthesis is accomplished via the aforementioned epitaxy, utilizing methods such as MBE or MOVPE. One particularly attractive option for NW and NWQD formation is the VLS growth mode, with two subcategories being identified, namely the foreign-metal catalyzed growth and the self-catalyzed growth. In both cases, a liquid catalyst seed acts as the collector and absorbs the feeding material. The incorporation of the elemental supply in the catalyst droplet eventually leads to supersaturation, which causes the nucleation of a solid crystal monolayer in the liquid/solid interface [43]. The continuation of this mechanism leads to NW elongation, i.e. the NW growth. QDs can be embedded axially via stacking a narrower bandgap material within the NW, which is achieved by controlling the material supply during growth. It is important to mention that the sharpness of QD/NW interfaces should be kept as abrupt as possible. The carriers are ideally confined in the narrower bandgap region (the QD), resulting in radiative recombination deriving from the QD region [44]. The emitted photons are guided by the NW to the ending facets. From there, they can be coupled with one of the fundamental modes of free space and collected for further processing [45]. In III–V NWQDs in particular, the dot formation can be achieved via altering either a group III [46, 47] or a group V element [48]. It is interesting to underline that apart from VLS mode, SAG is also another subcategory of bottom-up NW synthesis. According to this method, the substrate is patterned via the use of a patterned hard mask, EBL and etching. This way an array of meticulously regulated holes is presented on the substrate wafer, where NWs preferentially elongate. Despite the benefit of this method in terms of uniformity, the challenges related to the additional fabrication steps and the lack of thorough understanding of the underlying mechanisms significantly limits the use of SAG, especially in the case of NWQDs, where the existing literature is based on VLS, bottom-up growth. For the rest of the article, we will focus on VLS-grown NWQDs, which represent the cited literature to its entirety.

Ternary III–V NWQDs are obtained by foreign metal, most usually Au, as catalyst droplet with excellent results. The choice of Au is advantageous when compared with other metals such as Ag or Ni owing to its properties including thermal stability, chemical inertness, resistance to oxidation, and solubility of group III–V semiconductors in Au [49, 50]. Despite the good results reported, the use of foreign metal catalysts entails a risk of contamination via the formation of Au clusters on the substrates, introducing mid-gap energy states [51]. In addition, potential Au intermixing with the NW material can cause deep-trap levels that pose challenges to the compatibility with CMOS technology applications and drive electronics [52]. For this reason, a suggested alternative route for III–V NWQD synthesis has been the self-catalyzed VLS growth, where the element of the liquid droplet is a component of the NW itself. Besides this fundamental difference, the working principles are identical to the foreign-metal catalyzed growth. The basic challenge of the self-catalyzed growth mode is the sensitivity of the material to the growth parameters, requiring highly careful design and calibration. Nonetheless, the self-catalyzed technique has been employed for QDs embedding in standing NWs [53–56]. A schematic representation illustrating the growth mechanism is provided in figure 2. The elemental fluxes are shown as arrows and the corresponding atoms as spheres. The self-catalyzed growth utilizes a group III element as the catalyst droplet, which could compromise the chemical stability of the droplet itself, so that the alteration of group III fluxes feeding the droplet is challenging. On the contrary, the alteration of group V fluxes does not have a significant impact on the stability of the material system due to their low solubility in the group III droplet.

After having introduced the growth mechanisms that are employed, we will focus on the material platforms that have been exploited for the realization of ternary III–V NWQDs. In each case, the peculiarities in morphology, structure, optical properties, and growth methods will be investigated.

3. Ternary III-V NWQDs

The past decade has been marked by an increased interest in III–V NWQD structures due to their intense and spatially localized emission with a potential to be used as single photon sources. Considering the aforementioned benefits of ternary

III–V structures, particular attention has been paid to the synthesis of ternary III–V NWQDs whose emission range can be easily tuned by modulating the nominal composition of the alloys. The two subcategories that we will examine are NWQDs with binary QD segments (GaAs) and ternary QD segments. Eventually, due to the significance of the material platform, we find it important to introduce III-nitride-based NWQDs in a separate subsection at the end of the current chapter.

3.1. GaAs QDs in ternary III-V NWs

As one of the most widely explored and popular III–V alloys, GaAs has been incorporated as the active region material in ternary III–V NWQDs. The NW body, which is considered the barrier material, is comprised of a wider bandgap ternary alloy. The two most widely used alloys for such a purpose are AlGaAs and GaAsP, which will be examined separately in the current report.

AlGaAs has a bandgap ranging between 1.42 eV (GaAs) and 2.16 eV (AlAs), rendering it an ideal platform for red and near-infrared light emission. In addition, AlGaAs has an almost identical lattice constant with GaAs, which leads to its regular combination with the latter in NW core/shell configuration [57–59], and thus results in advancements in non-classical light sources with enhanced intensity and polarization [60, 61] and lasers [57, 62].

Due to their lattice match, GaAs QDs have been successfully embedded in standing AlGaAs NWs in the past, with optical emission occurring between 600 and 800 nm [63–68]. The QD segment manifests itself as an additional emission peak, with higher intensity due to the enhanced quantum confinement effect in the GaAs QD region. It is noted that the growth parameters are crucial for the applicability of the nanostructures. For instance, it has been shown that in MBE-grown AlGaAs/GaAs NWQDs, the intensity of the emission signal is strongly dependent on the growth temperature. Specifically, when the growth temperature is increased from 510 °C to 550 °C, the PL emission of both the dot and the wire is significantly weakened, while there is also a blueshift of the peak [67]. Moreover, Al content and its distribution in the NW body have an impact on the QD size, since increased Al presence at the QD/NW interface can alter the thickness of the bare GaAs QD segment. Ergo, both NW-related and QD-related emission peaks can be significantly influenced [67]. For this reason, modulation of the QD size allows for the dot emission to be kept at the same value even for samples with different Al content in the AlGaAs barrier [67]. A schematic representation of a single GaAs QD embedded in the core of an AlGaAs NW is exhibited in figure 3(a). The corresponding Ga and Al maps are shown in figures 3(b) and (c), respectively, where the red arrows mark a bright (dark) segment in the map of Ga (Al) that represents the formed QD [68]. Finally, the energy dispersive x-ray (EDX) measurements reveal the atomic content for Ga and Al at the scan positions of the NW, showing the characteristic peak in Ga and dip in Al at the dot segment, as presented in figure 3(d). It is noted that the percentage of Al in the GaAs QD segment should be ideally maintained at 0. In experimental applications, this can never be the case as Al residues can be presented in the GaAs segment as a result of the widely non-uniform elemental distribution. As a result, an important parameter that regulates the optical behavior of the NWQDs is the sharpness of the NW/dot interfaces, with efforts being made to keep elemental diffusion causing intermixing minimal.

On the other hand, the GaAsP material platform has been studied extensively over the past years, due to its wide bandgap tunability between 1.42 eV (GaAs) and 2.24 eV (GaP). It is noted that zinc-blende GaP has an indirect bandgap, whereas GaAsP demonstrates an indirect-to-direct transition at 44% P content [69]. The bandgap range of GaAsP-based nanostructures makes them ideal for solar cells on Si [9] and photocathodes for water-splitting devices [8]. In addition, the narrow bandgap nature of GaAsP material platform has attracted attention for the realization of green LEDs, addressing the well-known ‘green gap’ in such devices, deriving from the lack of suitability of adequate materials. It is important to clarify that despite their promising potential, the use of GaAsP NW-based devices for solving the ‘green gap’ in LEDs is far from being understood or fully implemented and research is ongoing.

Embedding single GaAs QDs in GaAsP NWs has been accomplished in the past, with intriguing optical features being presented. The NWQD structures display an enhanced intensity of the emission deriving from the QD segment. The QD formation can be validated via transmission electron microscopy (TEM) techniques, where it manifests itself as a brighter region. This is because in dark-field TEM, bright fractions correspond to abundance in the heavier element, which in this case is Ga. This is demonstrated in figure 3(e), where the dot segment is circled for clarity. Moreover, mapping of the corresponding regions can reveal the formation of the narrower bandgap segment via illustrating the elemental content. In figure 3(f), the combined mapping along with the individual maps for As, P and Ga show the lack of P in the dot region, while EDX measurements also indicate the existence of the GaAs QD. The scan along the NW axis (upper image, figure 3(g)) presents a characteristic dip in P and a peak in As at the high brightness region, which reveals the formation of the GaAs QD (below image, figure 3(g)) [53].

As mentioned earlier, the pronounced quantum confinement effect in the dot regions leads to distinctive features of the dot-related emission. This emission can be controlled via different techniques. The controllability is scrutinized in figure 4(a) via PL measurements of different structures of GaAs/AlGaAs dot-in-wires. The QDs are grown for different times of 5 s, 7 s and 15 s, with longer growth duration leading to lower emission energy (longer wavelength) of the corresponding peaks, due to the varying size of the formed GaAs QD [8]. In addition, the self-formation of an AlGaAs shell exhibited in AlGaAs NW growth [70–72] affects emission as it increases the Al content of the QD. Nevertheless, it

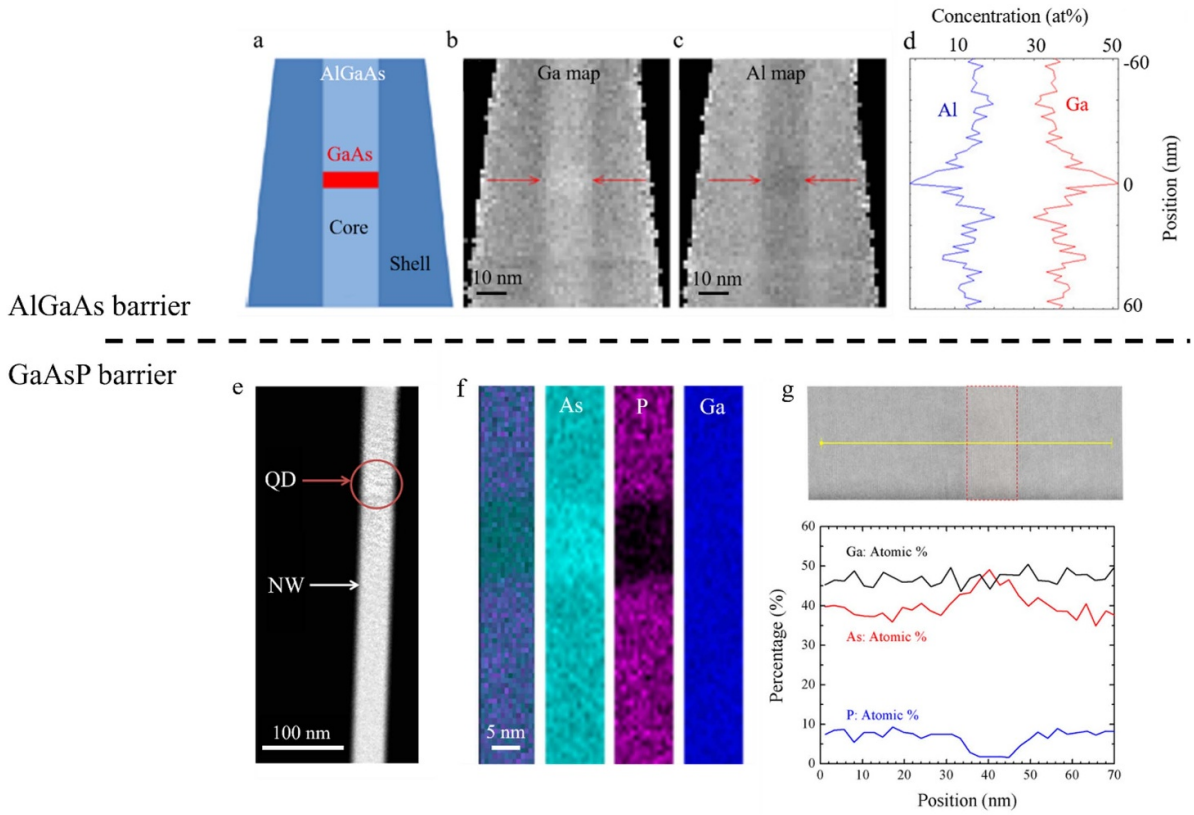

Figure 3. (a) Schematic representation of a single GaAs QD embedded in the axis of an AlGaAs core/shell NW. (b) and (c) Maps of Ga and Al, respectively, where the formed QD is exhibited as a bright segment in the former and a dark segment in the latter. (d) PL spectrum of three different structures where the dots were grown for varying times. Longer growth times signify higher dots and correspondingly lower intensity of the emission (higher wavelength). (a)–(d): Reprinted with permission from [68]. Copyright (2018) American Chemical Society. (e) EDX scan results for the NWQD in question at the dot region. The corresponding peak in Ga and dip in Al confirms the formation of the GaAs segment. (e) Dark field TEM of a GaAs dot embedded in a GaAsP NW, with the high brightness region corresponding to the former. (f) Elemental maps (combined, As, P and Ga, respectively) indicating the formation of the GaAs QD by the low P content. (g) Upper image: TEM of the dot region used for scanning along the yellow line. Below image: results of the scan showing the atomic percentages as a function of the position, revealing the peak in As and dip in P in the QD segment. (e)–(g): Reprinted with permission from [53]. Copyright (2016) American Chemical Society.

is important to maintain this Al presence at the lowest level possible to avoid increasingly shallow interfaces that would eventually cause non-negligible shifting of the emission peaks. Via adequate control of the parameters, ultra narrow emission peaks from GaAs QDs GaAs/AlGaAs core/shell NWs have been reported [73]. The linewidth of the peak, deriving from excitonic transition, does not exceed 315 μeV, while the biexciton-related peak at higher energies has a linewidth of 458 μeV (figure 4(b)). Besides, the low energy peak (X) presents a linear dependence with the excitation power, before saturating at 0.4 μW, while the high energy peak (X*) emerges at the onset of the X-peak saturation and has a superlinear dependence with the excitation power (figure 4(c)). Furthermore, time-resolved PL for the two peaks reveals that the decrease of the X* intensity corresponds to an increase of X at 0.25 ns, signifying that X* decays into the lower state X-peak (figure 4(d)). Based on the above, X* is assigned to higher charge states of a trion or a biexciton, while X is ascribed to an exciton transition. The reported values are compared to SKQD results [74]. Such NWQDs can be exploited for the realization of non-classical light sources with strong antibunching behavior. This is confirmed by second-order correlation (g^2) measurements via the Hanbury-Brown-Twiss (HBT) experiments, corroborating a g^2 at zero-time delay of 51% [73]. This is a key characteristic for quantum information processing applications.

It is interesting to point out that the majority of the AlGaAs/GaAs NWQDs are based on the Au-driven growth method [8, 9, 66–69], due to the inherently sharper QD/NW interface. Nevertheless, as mentioned earlier Au has the disadvantage of fast diffusion and the potential formation of deep level traps [49, 50]. Hence, the self-catalyzed growth method appears to be a suitable alternative. Despite its sensitivity in terms of growth conditions and its challenges in sharp interface formation, limiting the volume of the reported works, self-catalyzed growth is still considered the best alternative to avoid contamination and ensure compatibility with CMOS applications. This has been highlighted by recent achievements of self-catalyzed AlGaAs/GaAs NWQDs with good morphology and promising optical features [75, 76].

Considering that the GaAs QD segment remains the active region, similarly good optical response is observed in

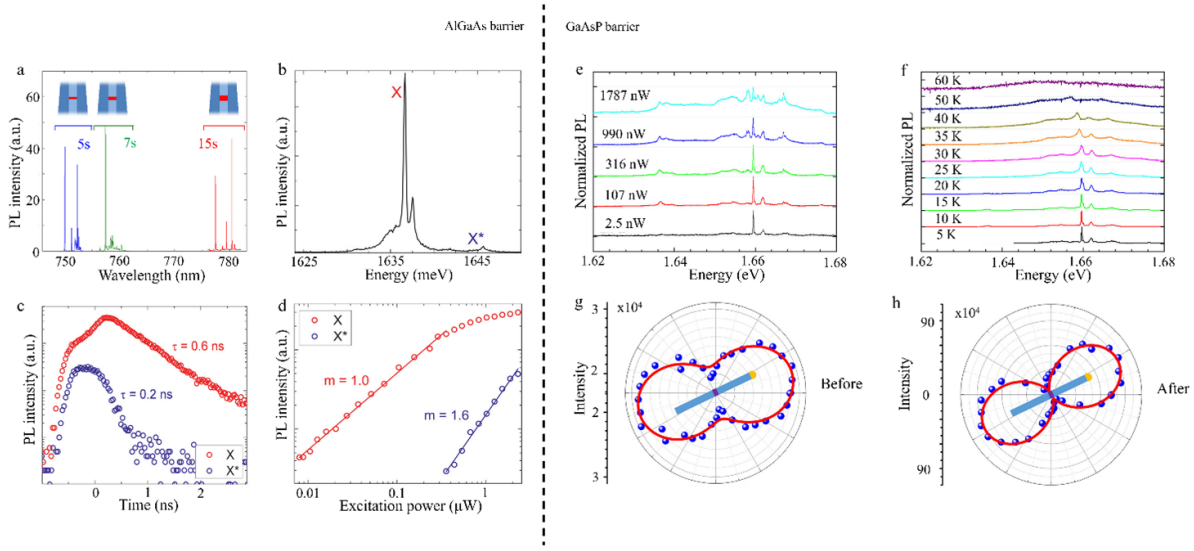

Figure 4. (a) PL spectrum of three different structures where the dots were grown for varying times. Longer growth times signify higher dots and correspondingly lower intensity of the emission (higher wavelength). (a): Reprinted with permission from [68]. Copyright (2018) American Chemical Society. (b) PL spectrum of GaAs QDs embedded in GaAs/AlGaAs core/shell NWs. Two peaks are presented ascribed to exciton (X) and either biexciton or trion (X^*) transitions with linewidths of 315 μeV and 458 μeV, respectively. (c) PL intensity as a function of the excitation power, showing linear dependence of X and superlinear dependence of X^*, further confirming excitonic transition for the former and higher energy state-related transition for the latter. (d) Time-resolved PL of the two peaks (X and X^*), where the decay of X^* to the lower charge state X is conspicuous. (b) –(d): Reprinted with permission from [73]. Copyright (2015) American Chemical Society. (e) and (f) Power-dependent and temperature-dependent PL spectra for a single GaAsP/GaAs NWQD, respectively, revealing a dot-related peak at 1.66 eV with a narrow linewidth, which disappears above 60 K. (e) and (f): Reprinted with permission from [53]. Copyright (2016) American Chemical Society. (g) and (h) Polar plots for GaAsP/GaAs NWQD emission before and after surface treatment, respectively, illustrating enhanced intensity and degree of polarization following the passivation techniques. (g) and (h): Reprinted with permission from [21]. Copyright (2019) American Chemical Society.

the case of GaAsP/GaAs NWQDs. The power-dependent and temperature-dependent PL spectra are shown in figures 4(e) and (f), respectively, where a sharp dot emission is presented at 1.66 eV (746 nm) with a linewidth of 130 μeV. The dot peak rapidly quenches with increasing temperature and practically vanishes after 60 K [53]. It is noted that, as in the case of AlGaAs NWs, the inhomogeneous elemental distribution and crystal defects allow for carriers to escape the GaAs dot and recombine in the NW body, thus leading to a GaAsP-related peak. However, this has a weaker intensity than the predominant QD emission. Moreover, NWQDs with good photon antibunching behavior up to 160 K and narrow transitions up to 220 K have been reported [21]. These have a much higher intensity and degree of polarization (DOP) following surface passivation, as illustrated in figures 4(g) and (h), representing polar plots before and after surface treatment, respectively. The highest DOP reaches 82.5%, which is promising for the wide-scale use of phosphides in optical communications [21].

It is worth noting that the spectral range of the emission for AlGaAs/GaAs and GaAsP/GaAs NWQDs is similar, despite the different materials used as barriers. This is obvious from the emission wavelength of figures 4(a) and (e), (f) for the 5 s grown QDs which is located around 750 nm roughly. On the contrary, stark differences are observed between NWQDs of the same material but with different growth times, as wider QDs lead to a distinct redshift of the emission wavelength. Moreover, the influence of post-growth surface treatment and passivation can be deduced from figures 4(g) and (h), where the optical response in terms of non-classical light emission is highly improved in passivated structures, owing to the reduction of non-radiative recombination in the frequently dense surface states. The above indicates that the growth parameters and processing steps are of grave significance for the optical response of the material system.

3.2. *InAsP QDs in InP NWs*

The second subcategory of our review is related to the growth of ternary III–V QDs acting as the active region in III–V NWs. Regarding that, one particularly interesting topic has been the formation of InP/InAsP NWQDs on InP (111)B substrates [77, 78]. InAsP has a bandgap between 0.36 eV (InAs) and 1.344 eV (InP), covering a wide range of the near- and mid-infrared regions of the spectrum. Moreover, its high electron mobility and large absorption coefficient are ideal properties for electronic applications [79]. Hence, InP/InAsP NWQDs are promising for bright and effective single photon emission. For instance, two InAsP QDs with different geometry have been embedded in InP NWs. The schematics are presented in figures 5(a) and (c), while the corresponding TEM images are shown in figures 5(b) and (d), respectively. The accomplished peaks have an ultra narrow linewidth of less than 120 μeV and are found at 1.401 and 1.412 μm, respectively (figure 5(e)). The sharpness of the peaks and the narrow linewidth reveal the QD-like behavior of InAsP insertions. Nevertheless, their

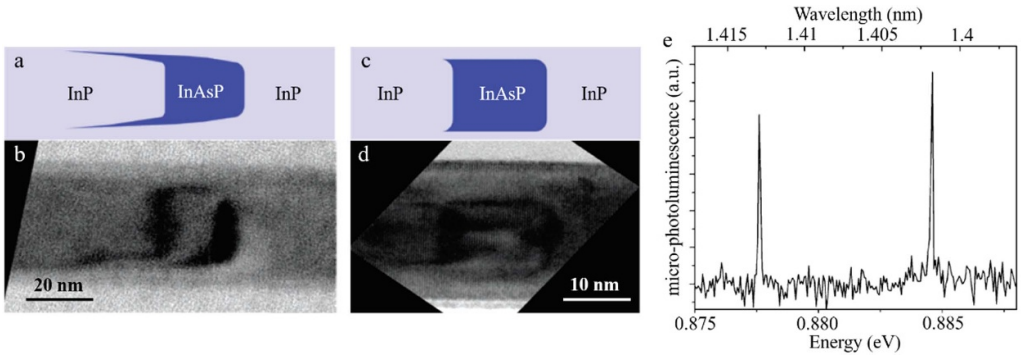

Figure 5. (a) Schematic representation of an InAsP insertion in an InP NW. (b) TEM image showing the shape of the insertions depicted in figure 4(a). (c) Schematic representation of a second InAsP insertion of a different shape in the same InP NW. (d) TEM showing the geometry of the InAsP insertion depicted in figure 4(c). (e) μPL spectrum of the InP/InAsP NW heterostructure with two insertions of different geometry. (a)–(e): Reprinted with permission from [77]. Copyright (2007) American Chemical Society.

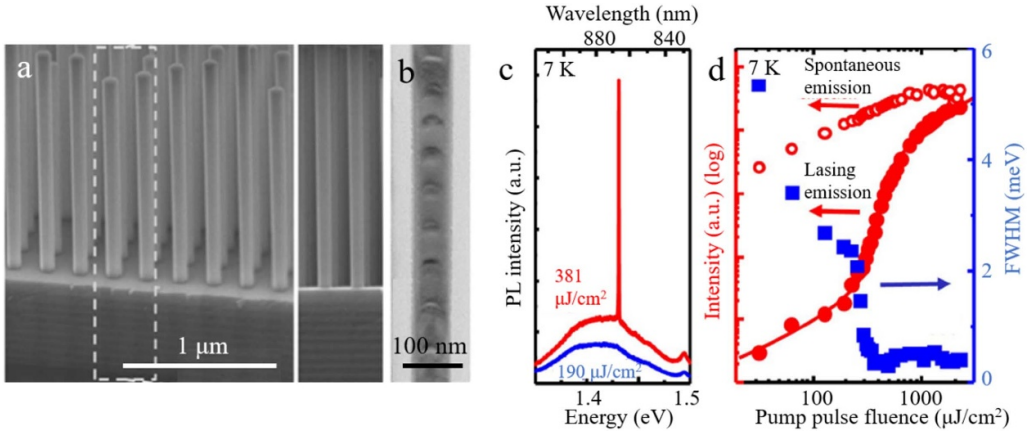

Figure 6. (a) SEM images of an array that includes GaAs NWs with InGaAs/GaAs QDs embedded. (b) Representative TEM image of a structure deriving from the array of (a), showing the existence of 75 QDs along the NW axis. (c) PL spectra of the structures in (a) and (b), below (blue) and above (red) the threshold pump pulse fluence (250 μJ cm^{-2}). The sharp peak at the latter indicates lasing. (d) Double logarithmic plot of the intensities of the peaks and the corresponding FWHM as a function of the pump pulse fluence. The S-shape behavior establishes a lasing trend. (a)–(d): Reprinted from [83], Copyright (2016), with permission from Elsevier.

shape is larger than conventional QDs, as their dimensions exceed the Bohr exciton radius [77]. Ergo, further optimization of the dimensions could lead to sharper peaks due to stronger quantum confinement. Furthermore, this material platform has shown tunability of the P content, varying between 20% and 100%. The insertion of InAsP QDs in InP NWs has been modeled as well, with vanishing fine-structure splitting [80]. Hence, the aforementioned observations can pave the route for the realization of entangled photon pair sources, which is a crucial step towards achieving photons of high indistinguishability and is therefore key to promoting the research related to quantum computing [81, 82].

3.3. InGaAs QDs in GaAs NWs

It is interesting to observe that embedding multiple QDs along the NW axis is of equal importance and has contributed to the fabrication of lasers. Specifically, InGaAs QDs embedded in standing NWs have shown remarkable results [25, 83–85]. For instance, the insertion of 75 InGaAs QDs in GaAs NWs has achieved laser oscillations at 1.43 eV with a threshold pump of 250 μJ cm^{-2} [83]. Typical SEM images of the aforementioned NWQDs are presented in figure 6(a), while the corresponding TEM is introduced in figure 6(b). Moreover, the PL spectra at 7 K of a single structure with stacked $In_{0.2}Ga_{0.8}As$/GaAs QDs below and above the threshold are shown in figure 6(c), where the sharp peak above the threshold indicates lasing. Besides, the logarithmic integrated output power intensities of the laser peak and the linewidth as a function of the pump pulse fluence exhibit the characteristic S-shape behavior that confirms laser realization (figure 6(d)) [83].

Besides, modulation of the emission energy of each QD in NWs via tailoring the size of the dot can be used to avoid inhomogeneous broadening, as it has been established that progressively shorter growth duration can lead to peaks as narrow as 9.3 me [84]. It has also been shown that the amount of QDs in a single NW could potentially reach 200 [84, 85]. One of the most important accomplishments of multiple QDs in NWs is the RT operating laser based on 50 $In_{0.22}Ga_{0.78}As$/GaAs QDs embedded in GaAs/$Al_{0.1}Ga_{0.9}As$/GaAs core/shell/cap NWs [25]. The QDs are separated by GaAs spacer layers. At low power densities,

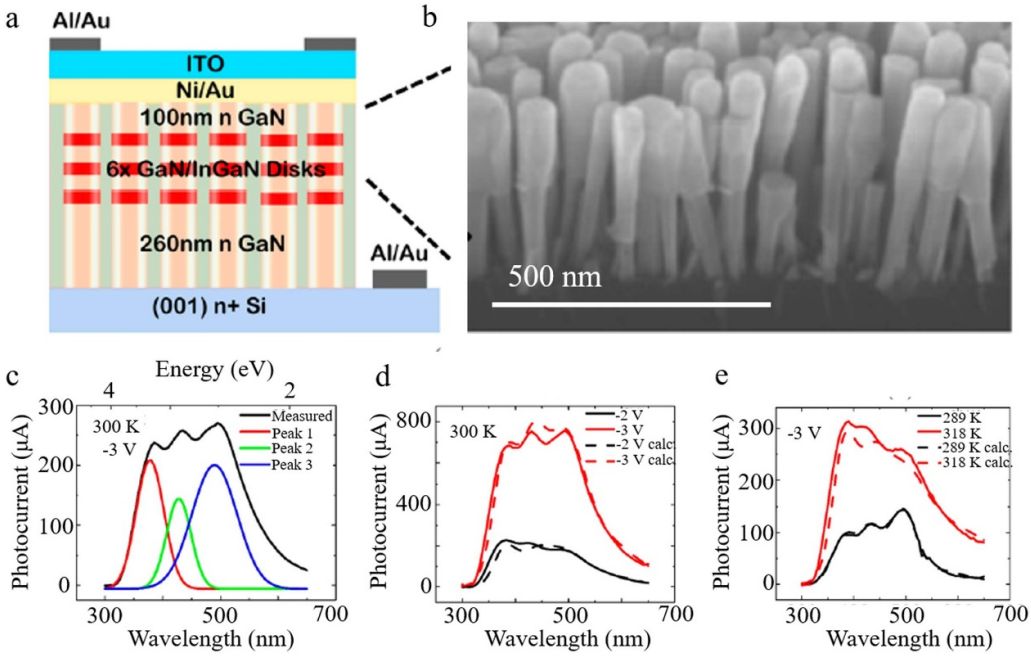

Figure 7. (a) Schematics of a GaN NW array with InGaN quantum disks that function as QDs embedded in their axis. (b) SEM image of the GaN/InGaN NWQD array, revealing a high density. (c) Photocurrent spectra of the fabricated photodetector exposing three different peaks. (d)–(e) Photocurrent spectra at varying bias voltage (d) and temperature (e) marking the strong dependence of the peak intensity on these two factors. (a)–(e): Reprinted with permission from [91]. Copyright (2019) American Chemical Society.

the emission is manifested as a broad peak due to the high density of the dots. Nevertheless, increasing power densities lead to another peak at 1.4 eV, with the threshold for lasing being at 25 μJ cm^{-2} after which a sudden jump in the peak intensity appears at 1.43 eV, indicative of stimulated emission. The transition from broad spontaneous emission to amplified spontaneous emission and eventually lasing is clearly exhibited in the *L–L* curve which presents a conspicuous S-shaped behavior [25]. Despite the fact that lasing at elevated temperatures is challenging due to the enhanced mobility of the carriers and the inhomogeneous broadening as a result of the enhanced thermal energy, clear stimulated emission is produced even at 300 K in the current example, which is ideal for fully operating lasers in real-time applications [25].

3.4. III-nitride NWQDs

Following the description of III–V material platforms for NWQD synthesis, the reported results on ternary III-nitride (III-N) NWQDs have drawn much attention. Group III-nitrides have emerged as a promising platform in NW growth due to their unique properties that are challenging to address by means of other semiconductor platforms, most notably their bandgap tunability from the infrared to the deep ultraviolet region of the spectrum [86]. Moreover, their high dielectric breakdown voltage, high thermal conductivity and high thermal and chemical stability have led to their implementation in a wide range of electronic applications including high-frequency transistors, wireless communications and switching systems [86]. Nonetheless, their most notable use is in solid-state lighting sources such as UV lasers and LEDs [87, 88]. Moreover, GaN QDs have exhibited one of the highest single photon purities recorded [89]. Due to their interest in nanotechnology applications, we will examine this unique type of semiconductor materials in NWQD synthesis in this separate section.

The main focus of existing literature is InGaN/GaN NWQDs [90–93]. A characteristic example of the progress related to this topic is the InGaN quantum disks in GaN NWs monolithically integrated on Si. The study reveals that the InGaN region acting as QD produces sharp excitonic transitions due to the pronounced quantum confinement effect, implying a high probability of single photon emission [90]. Moreover, the insertion of InGaN QDs in an array of GaN NWs has been used for photodetector fabrication with exceptionally high gain [91]. A schematic representation of the above is elucidated in figure 7(a), while the SEM image of the highly dense NW ensemble is provided in figure 7(b) [91]. After fabrication, the photocurrent spectra at RT and a bias of −3 V (figure 7(c)) demonstrate three distinct peaks, attributed to interband absorption [91]. In addition, the intensity is dependent on the bias and the temperature. Specifically, the varying bias of −2 V and −3 V at RT (figure 7(d)) shows that the intensity of the peaks is largely reduced at −2 V. Moreover, the spectra at 289 K and 318 K with −3 V bias reveal that the intensity is improved with increasing temperature, highlighting the suitability of the photodetectors for RT functionality [91]. On the other hand, single InGaN QDs of 2 nm width embedded in GaN NWs with a p-n junction have presented good optical properties, with the intensity of the dot-related peak being very high and being maintained even up to room temperature (RT), while the μPL

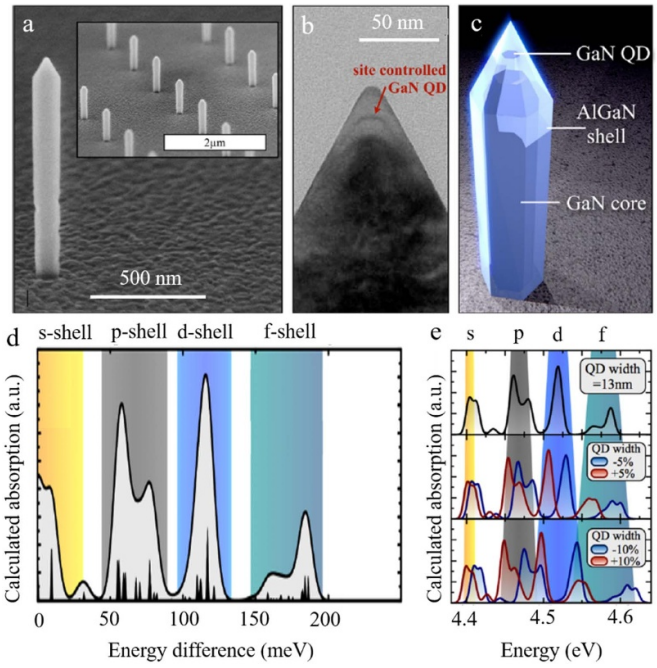

Figure 8. (a) Outset: SEM of an individual GaN/AlGaN core/shell NW with a GaN QD embedded close to the tip. Inset: SEM of a wider area of the sample. (b) TEM image of the tip of the NWQD presented in (a). The bright region reveals the QD formation and is marked by the red arrow. (c) Schematics of the intricate nanostructure of (a) and (b). (a)–(c): Reprinted with permission from [94]. Copyright (2014) American Chemical Society. (d) Calculated absorption spectrum for s-, p-, d- and f-states of the shell of a GaN/AlGaN core/shell NW with a GaN QD embedded at the tip. The QD width is 13 nm. (e) Calculated absorption spectra of the same structure with varying dimensions of the QD. (d) and (e): Reprinted with permission from [95]. Copyright (2015) American Chemical Society.

of an individual NWQD reveals an exciton and a biexciton transition [93].

Moreover, III-nitride material platform has been used for the realization of more complex systems and structural morphologies. One example of an intricate structure that is formed is an embedded GaN QD in the tip of the AlGaN shell surrounding a pyramidal GaN [94]. A representative SEM image is provided in figure 8(a), with an individual structure shown in the outset and a wider area of the sample in the inset, while the corresponding TEM and schematics are illustrated in figures 8(b) and (c), respectively. The bright region in the pyramidal tip (figure 8(b)) signifies the GaN QD [94]. Furthermore, the excited states of individual QDs were probed by photoluminescence excitation (PLE) spectroscopy at 4 K. The continuum of states was centered at 4.42 eV [95]. However, the spectrum was comprised of several individual transitions at various energy levels above the ground state, which correspond to the different excited energy states [95]. For several different samples, it has been concluded that the ground state energy is located at 4.4 eV, while the excited state-related emission begins at 70 meV above the ground state energy. Apart from the aforementioned experimental procedure, nextnano simulations also unveiled details of the electronic structure of the GaN QDs embedded in GaN/AlGaN NWs. The shell structure has been identified, with s-, p-, d- and f-states-related peaks being displayed in the calculated absorption spectra of figure 8(d) [95]. The sharp lines suggest individual transitions, while the energetic bunching of electron states is shown by the calculated energies of each shell state. Moreover, spectra for assorted sizes of QDs are shown in figure 8(e), where it can be observed that modifications in the dot size cause severe shifts in the excited-state separations, establishing that excited and ground state energies can be efficiently modulated via altering the QD dimensions [95].

Finally, InGaN QDs with 20% In content have been embedded in AlGaN NWs, leading to single photon emission in the blue region of the spectrum and a noticeably short radiative lifetime of 0.7 ns and highly polarized emission [96].

3.5. Role of modeling in ternary III-V NWQDs

Based on the analysis conducted in the previous sections of the current review, it has been demonstrated that the design of nanostructures is vital for their successful optical response and their potential for wide-scale implementation in novel devices. For instance, in the case of NWs, the morphology and structural properties of the core and the shell along with the compositional variations and control of the elemental distribution are some of the most important factors in terms of the NW functionality. Moreover, one of the most interesting features of NWs, hence of NWQDs as well, is the polytypic nature, meaning that unlike bulk materials NWs can be crystallized into either the cubic ZB or the hexagonal WZ phase. In addition, interestingly, a combination of the two phases can co-exist within the crystal leading to mixed-phase NWs, an example typically observed in the majority of ternary NWQDs. Due to the importance in the design of the structures and the subsequent determination of growth parameters to achieve them, theoretical modeling and simulations have played an important role. Therefore, even though an extended analysis of the theory and the principles behind it is outside the scope of the current review, it is important to introduce the significance of simulations in the regulation of the optoelectronic properties of ternary III–V NWs and NWQDs [97–102].

As mentioned earlier, controlling or predicting the properties of NWs based on the phase they are crystallized into, has been the main focal point of research in theoretical model development. Using density functional theory (DFT) and the GW approximation has been the most popular tool in numerical calculations that allowed for the determination of electronic and optical properties of NWQDs in either the WZ or the ZB phase. For instance, numerical modeling of AlGaAs/GaAs NWQDs utilizing the aforementioned approximations enabled the study of polymorph WZ/ZB cylindrical shape AlGaAs NWs with single GaAs QDs embedded [97]. The results showed small but non-negligible strain field generated in the WZ/ZB interfaces within the AlGaAs crystal, as anticipated [97]. Moreover, the analysis of the confined energy levels showed clear signs of blueshift of the emission in WZ regions as opposed to ZB regions, actively showing that the synthesis of WZ AlGaAs NWs exhibits distinct interest in reaping

novel AlGaAs-related optical properties [97]. What is more, band-structure calculations in AlGaAs NWs performed with a multiband $k\,p$ model [98], have strongly suggested that WZ AlGaAs is direct bandgap material for high Al concentrations [99]. It is reminded that ZB AlGaAs remains direct bandgap only for Al contents up to 60%. The bandgap of WZ AlAs (2.232 eV) has also been numerically calculated. Moreover, the comparison between PL experimental data and theoretical, numerical simulations confirm the validity of the aforementioned method.

The above demonstrate the importance of WZ AlGaAs synthesis, as higher Al content while maintaining optically active properties can allow for stronger barrier layers, hence higher quantum confinement and sharper interfaces in AlGaAs/GaAs NWQDs. This can circumvent one of the main obstacles of RT operation which is carrier escape, as will be analyzed later on in the current review. The above have been recently confirmed via direct numerical calculations using the same model in AlGaAs/GaAs single NWQDs. It has been shown that the level of quantum confinement when using WZ Al-rich AlGaAs layers is strong [100]. Specifically, the quantum confined Stark effect observed in the case of WZ AlGaAs has a dramatic impact on the optical properties of the dot itself, via modifying the quantum confinement level, the carrier escape and via drastically reducing wavefunction overlap [100].

It is interesting to mention that a change in the size of the dot has also been predicted to significantly shift the emission energy via modifying the quantum confinement levels in the dot region. This has been experimentally applied as well via modifying the growth time of the GaAs segment [68]. A comparison of the simulated transition peaks and the PL experimental data are shown in figure 9. Despite the difference in the intensities, which derive from competing charging mechanisms under non-resonant excitation in experimental PL [100], there is an excellent agreement in the spatial localization of the peaks, confirming the validity of the mechanism.

After having analyzed the experimental data and briefly showed the role of numerical calculations in NWQD design, it is important to proceed in the next section in the analysis and measurements of ternary III–V NWQDs acting as single photon sources, with the aim to be used in novel quantum information processing applications.

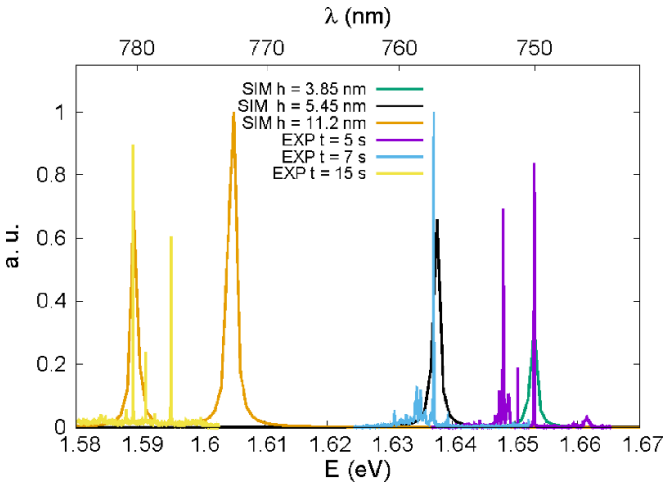

Figure 9. Experimental (EXP) PL under different growth times of the dot, compared to simulated, numerical data (SIM) under different dot sizes. The good agreement of the position of the peaks confirm the validity of the proposed model. Reproduced from [100]. CC BY 4.0.

4. Ternary III–V NWQDs as single photon sources for quantum information processing applications

4.1. Single photon emission in NWQDs

One of the unique features of QDs is single photon generation stemming from the strong carrier confinement. Single photon sources are vital for the development of quantum computing because the emitted photons play the role of single qubits, as the carriers of quantum information. As mentioned in the introduction, single photon generation offers the advantages of high brightness and interconnectivity [30]. What is more, a high level of indistinguishability is essential for quantum computing applications [31, 32]. Among the achievements of the past decade on quantum information processing, the realization of quantum-controlled NOT gates [32, 33] and multiqubit entanglement gates [34] exhibit the scalability and practicality of quantum computing as an emerging technological advancement.

To ascertain single photon emission, the most popular and reliable technique is the HBT experiment, which is fundamentally comprised of a coherent light source, a beam splitter and two photodetectors. The main aim of the experiment is the measurement of the correlation of the two photons that are detected by the two individual photodetectors. This is accomplished via measuring the second-order correlation function ($g^2(\tau)$), where τ is the time delay between the two detected photons. More specifically, $g^2(\tau)$ provides the degree of correlation between the photon detected at the initial time t and the delayed time $t+\tau$. The most important value for single photon generation is $g^2(0)$, which essentially defines the possibility of two photons being detected (thus emitted) simultaneously. In principle, this value needs to be maintained at low levels, ideally 0 [103]. Practically, the threshold to corroborate single photon emission is $g^2(0)$ to be less than 0.5. This is a property exhibited in QDs in the past, with an ultralow possibility of the second photon being emitted at the same time [89, 104]. For example, high purity has been accomplished in GaN QDs, with ultralow $g^2(0)$ of 0.02 [89]. A schematic representation of a typical HBT setup is presented in figure 10.

Nevertheless, the difficulties related to the complexity of QD formation along with the increasing need for versatile structures led to the quest for an alternative route in single photon generation. On that regard, NWs can play a pivotal role. It is important to clarify that NWs do not inherently function as single photon emitters, as NW emission is frequently characterized by inhomogeneous broadening due to alloy fluctuations, while the peak intensity does not reach the high values

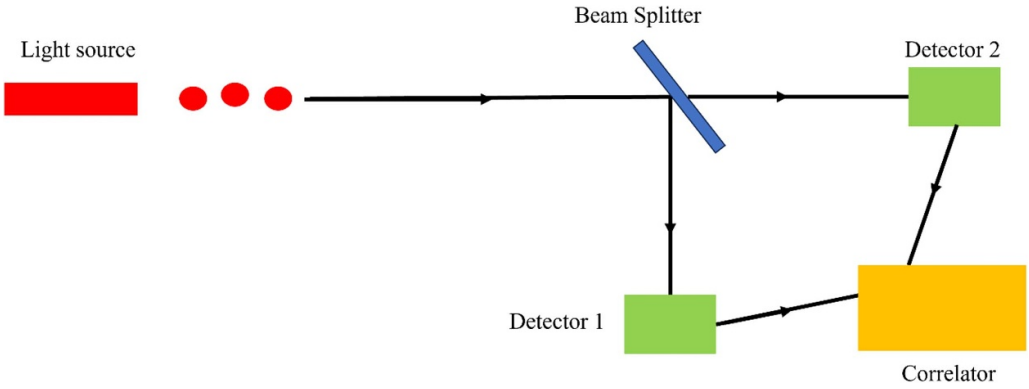

Figure 10. Schematic diagram of a typical HBT setup consisting of a light source, a beam splitter, two detectors and a correlator for the measurements of g^2.

of QD emission often, due to the less accentuated quantum confinement. In addition, the high surface-to-volume ratio of NWs leads to a profound impact of highly dense surface states that function as scattering centers for carriers and compromise the intensity of the NW emission.

Opposite to this, axially embedded QDs in NWs exhibit significant advantages. First and foremost, the narrower bandgap material stacked on-axis demonstrates 3D carrier confinement resulting in sharper peaks. Furthermore, the 0D nature of the QD allows for narrow linewidth, thus enabling single photon generation. It is interesting to underline that the above are features of conventional QDs in terms of single photon emission. Nevertheless, the advantages of NWQDs are mostly related to the nature of the NW structures. The large strain tolerance allows for the combination of materials without the need of intricate buffer design and fabrication, facilitating the growth process. Simultaneously, the high density of surface states can be addressed by adequate passivation. Besides, QDs are deterministically positioned in the NW, as opposed to strain-driven SK QDs, which allows for a high-level controllability in the structural design. Most importantly, NWs inherently act as waveguides for the emission that derives from the QD segment, which is of foremost importance for the efficient collection and manipulation of the emission from the ending facets. Hence, QDs embedded in NWs are considered beneficial as single photon sources.

4.2. Ternary III–V NWQD-based single photon emitters

One of the main platforms for successful single photon emission has been ternary III–V NWQDs, due to the optically active properties that were analyzed earlier in the current review. Among the many material systems GaAs/AlGaAs manifests itself as an ideal combination, as both GaAs and AlGaAs have near-identical lattice constants, signifying that minimal strain is introduced in the interfaces. This is important owing to the resulting reduction of intermixing and necessary interface sharpness. Despite the importance of GaAs/AlGaAs material platform, it is important to underline that successful results on single photon generation from NWQD-based systems are quite limited for the aforementioned alloy combination. This is potentially due to the complexities associated with Al distribution. Specifically, Al tends to incorporate at the bottom facets of the NW leading to wide variations of the compositional distribution along the NW axis. In addition, the mixed crystal phase of AlGaAs-based NWs further increases the intricacy of the nanostructures. Hence, achieving an adequately low $g^2(0)$ has been challenging. Nevertheless, single crystal phase GaAs QDs embedded in GaAs/AlGaAs NWs have exhibited a $g^2(0)$ of 51% [70]. Even though this value can only indicate marginal single photon generation, it strongly suggests photon antibunching.

Based on the above, it is suspected that crystal quality optimization and reduction of alloy fluctuations can lead to lower $g^2(0)$ and allow us to reap the benefits of the AlGaAs/GaAs material system in terms of non-classical light generation. Specifically, using higher Al content can increases thermal stability which in turn widens the frame of growth temperature optimization. Moreover, stability that can be obtained ex-situ via other tools can support the extensive use of AlGaAs/GaAs NWQDs as single photon sources. For example, single GaAs QDs in Au-catalyzed AlGaAs NWs, whose emission has been tuned ex-situ to atomic resonances under the influence of Rubidium, have shown excellent photon antibunching [68]. This is achieved by directing the emission deriving from the QD to a Rb vapor cell and applying a varying magnetic field through which the frequency of the emitted photons is changed. Consequently, the photons propagate through the Rb cell, and they get absorbed or scattered [68]. This greatly lowered $g^2(0)$ down to 19%, which demonstrates single photon generation. It is important to underline that narrow linewidth in the PL spectrum is a strong first indication of photon antibunching. In [68] the exciton linewidth is maintained at 30 μeV, as illustrated in the spectrum of figure 11(a). The final confirmation of single photon emission derives from the aforementioned $g^2(0)$ whose low value validates the purity of single photons (figure 11(b)) [68].

Furthermore, reliable results have been observed in GaAsP/GaAs NWQDs [21]. Figure 11(c) demonstrates the g^2 measurements on bare NWQDs before any surface passivation

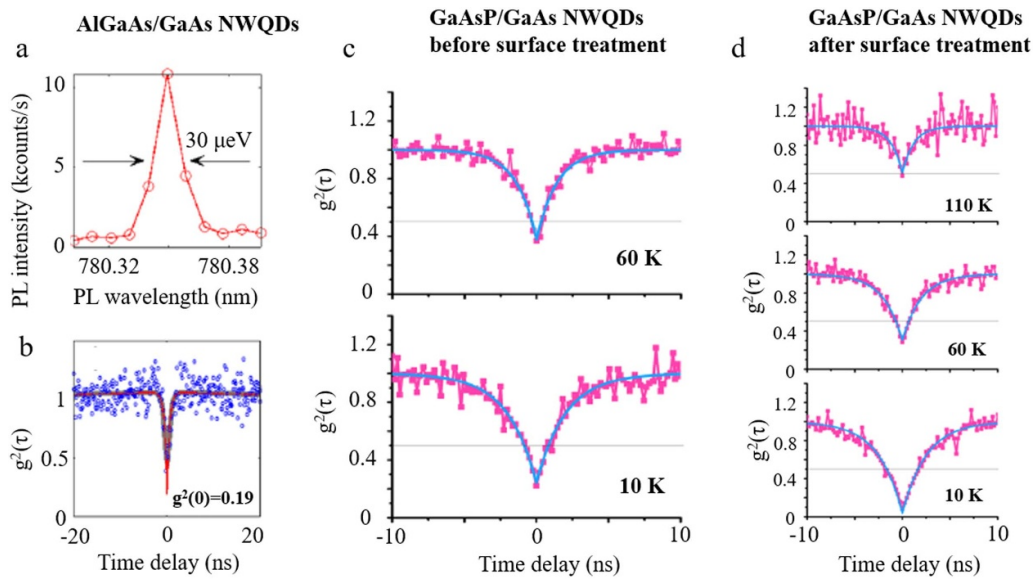

Figure 11. (a) PL spectrum of an exciton transition from a single AlGaAs/GaAs NWQD. The linewidth is narrow at only 30 μeV. (b) Second-order correlation function measurements from the same AlGaAs/GaAs NWQD. The large dip at zero-time delay with a value of barely 19% establishes single photon emission. (a) and (b): Reprinted with permission from [68]. Copyright (2018) American Chemical Society. (c) and (d) Second-order correlation function measurements from a single GaAsP/GaAs NWQD before and after surface treatment, respectively. The dip at zero-time delay, below 50%, corroborates single photon emission. Before surface treatment, the phenomenon is quenched at 60 K, while after surface treatment improved thermal stability is displayed with $g^2(0)$ being maintained at the relatively low value of 32% even at 110 K. (c) and (d): Reprinted with permission from [21]. Copyright (2019) American Chemical Society.

is performed. The results show a large dip at zero-time delay at 10 K (lower panel) and 60 K (upper panel). The value is below 50% in both cases, confirming single photon emission. However, the possibility of a second photon being emitted simultaneously is largely enhanced with increasing temperature due to the increased carrier mobility. After surface treatment is applied (figure 11(d)), the thermal stability is highly improved, with the dip being much more pronounced at 10 K (lower panel) and 60 K (middle panel), while signs of single photon emission are shown even at the elevated temperature of 110 K (upper panel). The values of $g^2(0)$ are 5%, 19% and 32% for 10 K, 60 K and 110 K, respectively. It is noted that a $g^2(0)$ of 48% was observed at even 160 K (not shown here), which is still below the critical value of single photon generation [21]. The above are important steps towards obtaining single photon sources, thus functional quantum computing at higher temperatures.

4.3. Ternary III-nitride NWQD-based single photon emitters

Significant results of single photon emission have been observed in ternary III-nitride NWQDs. The interesting properties of nitride material platform, combined with the NWQD architecture and the described features that they possess has allowed for the circumvention of two major obstacles that are exhibited in NWQD-based technology in terms of quantum light emission, namely RT operation and electrical pumping of the structures. In terms of the former, maintaining an adequately low $g^2(0)$ at increasing temperature has been the subject of intense scrutiny and is considered a key challenge in the wide-scale implementation of such structures. The deterioration of $g^2(0)$ measurements at RT operation has been the case in several NWQD reports on different material systems [105–107]. Nevertheless, the use of a wide bandgap system such as GaN/AlGaN with site-controlled dots [94] has led to important results in single photon emission, with the $g^2(0)$ remaining at a level of 33% even at 300 K operation [94]. The schematic representation of the structure with the site-controlled GaN QD in the AlGaN shell of a NW was already demonstrated in figure 8(c). In figures 12(a)–(c) below, we present the exhibited $g^2(0)$ graphs at different temperatures starting at 3.9 K (figure 12(a)) and being increased to 150 K (figure 12(b)) and 300 K (figure 12(c)) with the characteristic zero-time delay showing clear signs of single photon generation and antibunching behavior, as $g^2(0)$ remains at a low level of 12%, 14% and 13%, respectively. The non-zero value can be attributed to fast carrier repopulation and emission from the dot region [94].

It is interesting to underline that this sustainability of RT function is characteristic of III-nitride QDs [107] and can be attributed to the nitride inherent properties such as the strong built-in electric field that pushes the electrons at the top of the pyramidal QDs while holes remain at the bottom. This combined with the strain-induced piezoelectric field leads to strong carrier confinement that allows sustainability of RT operation even in challenging applications such as single photon emission [107]. Hence, the first fundamental reason of solving the RT associated issues is the material platform, which due to the wide bandgap and aforementioned properties enables exciton confinement at elevated temperatures. Moreover, it is

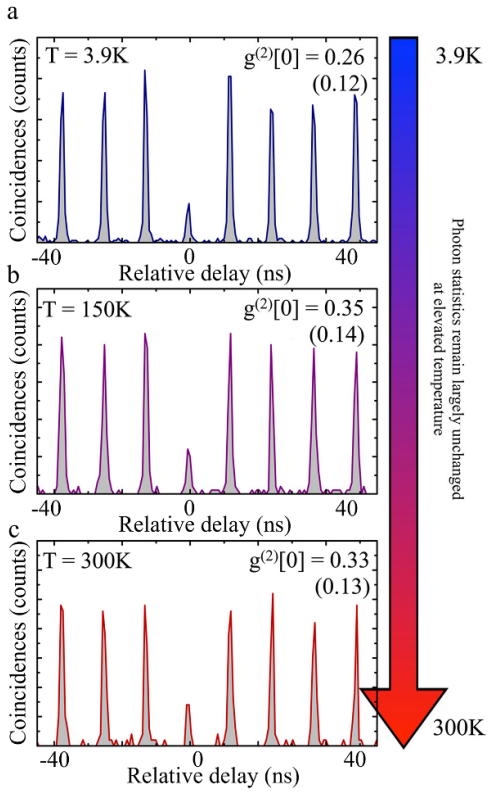

Figure 12. (a)–(c) Second order correlation function at zero-time delay for GaN/InGaN NWQDs at 3.9 K, 150 K and 300 K, respectively. Reprinted with permission from [94]. Copyright (2014) American Chemical Society.

interesting to point out that in the described report they used very small and site-controlled dots, which has a twofold consequence. First, it eliminates emission overlap from neighboring QDs and second, it enhances energy separation of the excited states, hindering spectral contamination from excited states of the same dot [95].

Apart from RT functionality, another important challenge that has been addressed with the use of III-nitride material system in NWQD single photon sources is the electrical injection, which essentially involves the formation of a p-n junction in the NW region. Similar to RT operation, electrically driven applications are key for practical wide-scale implementation of the structures and their integration into a large network, which is the final aim of scientific research [108]. Hence, scalability is a prerequisite and is challenging to achieve in bulk optical systems, where usually there is the need for a high power laser as an excitation source and many various components. Moreover, electrically driven structures and devices allow for highly precise control of the emission, rendering the structures suitable for practical implementation in industrial demands [108]. Nonetheless, electrically driven single photon sources suffer from major challenges. First, the QDs are embedded in a planar matrix signifying that light extraction efficiency is poorer at higher temperature, where carriers thermally escape the dot region. In addition to this, the large built-in electric field can have a strong impact in the radiative recombination process [109].

On that regard, III-nitrides exhibit distinct advantages such as the low surface recombination velocity [110], lack of strain and high material quality associated with the epitaxial nature of the growth. Hence, advancements have been made in the synthesis of electrically injected single photon sources based on GaN/InGaN material platform [93, 109]. For example in the investigated case of InGaN QD embedded in GaN NW, the top region is p-type and the bottom region n-type after Mg and Si doping, respectively [93]. The structure was subjected to *I–V* characterization, showing an ultrasmall reverse current of 1 pA and no breakdown up to a reverse bias of 20 V [93]. Electroluminescence measurements were conducted, showing sharp resonances and a distinct peak at 2.84 eV. At higher injection currents a second peak arises at 2.85 eV, increasing quadratically with the injection current, strongly indicating that the two resonances derive from single exciton and biexciton transitions, respectively [93]. Eventually, confirmation of single photon generation is the direct result of HBT experiment, as discussed earlier. The $g^2(0)$ for the two aforementioned transitions are 16% and 25% for exciton and biexciton transitions. These values clearly confirm photon purity and single photon generation, under electrical injection, which is an important step for industrial applications. Nevertheless, it is important to underline that the above experiments were conducted at 10 K, due to the previously described limitations of RT operation.

After having described the details on the material systems for the synthesis of NWQDs and their role in single photon generation in the previous chapters, it is important to present a table encapsulating the results and providing with a summary of the material systems and their basic characteristics as described earlier. The table 1 can be found below.

5. Ternary III–V NWQD single photon sources in quantum photonic circuits

Apart from their role in single photon emission, QD-based structures have shown wide potential for the realization of novel application related to quantum computing such as quantum key distribution [98] and 3D quantum networks [110]. For these reasons, it is equally important to investigate the functionality of our examined NWQD structures in quantum photonic circuits, which demand scalability and on-chip integration of non-classical light sources. Nevertheless, there are profound obstacles posing limitations to the wide-scale, commercialization of such compounds. The challenges lie in three fundamental aspects, namely generation, detection, and transmission. For instance, achieving an adequately high single photon brightness is a major focal point in terms of quantum light generation. On the other hand, the inevitable waveguide losses can render both detection and transmission challenging [111]. The above pronounces the need for effective coupling of the generated light to adequate waveguides with minimal losses to improve the aforementioned figures of merit. Accordingly, a significant amount of attention has been devoted to single photon generation, detection, and transmission, as well as effective coupling in quantum

Table 1. Encapsulation of the cited material combinations, the emission wavelength, second order correlation function and basic features.

Nanowire alloy	Quantum dot alloy	Emission wavelength	$g^2(0)$	Features
AlGaAs	GaAs	750–780 nm	19% at low temperature	Tunable emission, narrow exciton transition of 30 μeV
GaAsP	GaAs	∼750 nm	5% at low temperature	Polarized emission, sustained up to 220 K, narrow linewidth of 130 μeV
GaAs	InGaAs	870 nm	N/A (laser function)	75 QDs for lasing, threshold pump at 250 μJ cm^{-2}, room temperature operation
InP	InAsP	∼1.4 μm	13%	Fabrication of on-chip devices in quantum photonic circuits
GaN	InGaN	435–440 nm	16%	Room temperature operation, electrically driven devices

photonic circuits, with the results being milestones in up-to-date research.

Before analysing the parameters and architectures of the on-chip ternary III–V NWQD-based single photon sources and their role in quantum photonic circuits, it is interesting to describe some fundamental means of fabrication and processing steps that are essential. The basic principle lies on the transfer of a preselected NW to the waveguide, which happens using a nanomanipulator tool [112–116]. This tool usually consists of a tungsten tip mounted on a movable stage, while a high resolution optical microscope is used to visualize the stage and the sample. The van der Waals forces allow for the selected NW to adhere to the tungsten tip and to be transferred on the fabricated Si chip [112]. Interestingly, the level of accuracy in the positioning is high signifying that this method serves the purpose of the carefully deterministic positioning of the NWQD in the waveguide system. As far as the latter is concerned, the usual choice of material is SiN_x, while the chip usually consists of a SiO_x layer between the Si substrate and the waveguide, acting as buffer [112, 115, 116]. Widely used EBL, metal evaporation and lift-off serve as the means to create metallic structures such as heaters and marker fields on the oxide to complete the chip fabrication [116]. An additional, important processing step is the encapsulation of the active material, which in this case is the NWQD structure, in the SiN waveguide, which occurs via SiN_x deposition usually under plasma-enhanced chemical vapor deposition. Eventually, after transferring the features to the SiN_x, the SiN_x layer is etched, followed by a thorough cleaning process [115, 116]. The last step is the full coverage of the devices with a thick (1 μm) PMMA layer, which ensures symmetric mode confinement [112, 116]. It is interesting to underline that in several cases the fabrication occurs directly on piezoelectric crystal substrates (such as lead magnesium niobate-lead titanate crystals) which ensures strain tuning, allowing modulation of the QD spectral emission [115].

One of the most fundamental aspects in terms of quantum photonic circuit function is the coupling of the emitted light to the waveguide to minimize losses. This has been demonstrated by the remarkable coupling efficiency of high-purity single photon emission deriving from III–V NWQDs to SiN waveguides [112]. The most prevailing method that has been adopted for coupling of the photonic crystal waveguide single photon source is evanescent coupling. Specifically, the careful positioning of a tapered III–V NWQD on top of a waveguide has been proven to enable the effective transfer of the QD emission to the waveguide. This has been exploited for the coupling of InP/InAsP NWQDs to a SiN ridge waveguide with 74% efficiency [113]. Notably, the deterministic nature of the QD and the position of the NW on the waveguide allows for the fabrication of intricate quantum photonic circuits [113]. A schematic representation of the above is shown in figure 13(a). The same material platform has been used in the fabrication of highly uniform NW arrays, with a fabrication yield of 100% and a collection efficiency of 83% [114]. In the aforementioned cases, single photon purity was maintained, with very low $g^2(0)$, as presented in the example of figure 13(b) [114].

In terms of single photon sources, the optically active nature of III–V semiconductors along with the 1D nature of NWQD configuration and the impact of waveguide effect as described in the previous sections of the current article, allow for the employment of III–V NWQDs as single photon emitters in quantum photonic circuits with high purity and high brightness having been observed. The two most basic fundamental aspects for the choice of the aforementioned structures are the deterministic positioning of QDs in the NW acting as a waveguide and the high coupling efficiency of the dot-related emission to the waveguide that is attributed to the geometrical characteristics of the NW. Indeed, the propagation of carriers along the NW axis enables for the coupling of the NWQD emission to one of the fundamental modes of free space, which in turn makes measurements and manipulation of the emission less complex and more effective [39].

Besides, it is important to mention that apart from single photon generation and transmission via coupling with the selected waveguide, another integral function of quantum photonic circuits is the system's capability of on-chip detection of single photons. In that regard, it is essential to separate individual QD transitions via on-chip spectral filtering [116]. Specifically, it is key for the realization of intricate and multifunctioning quantum photonic circuits to selectively sequester optically active QD transitions deriving from multiple single

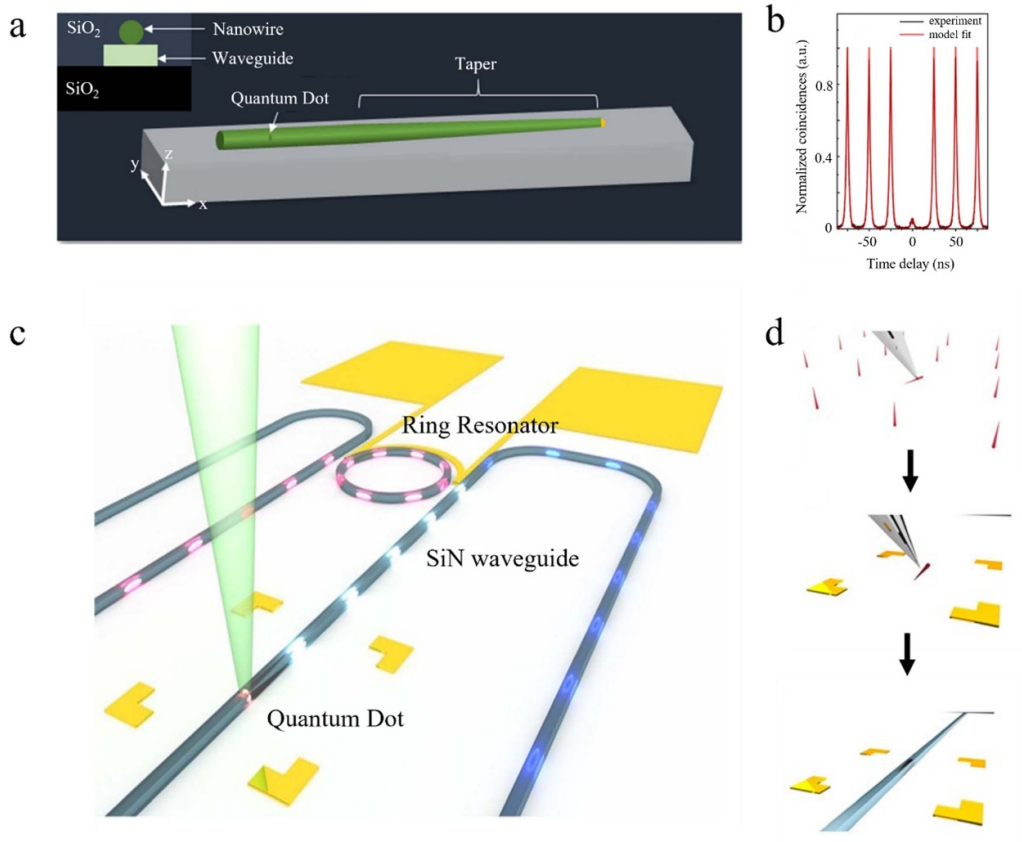

Figure 13. (a) Schematic representation of the InAsP/InP dot-in-wire structure integrated with the SiN waveguide, in a horizontal layout. [114] John Wiley & Sons. [© 2019 WILEY-VCH Verlag GmbH & Co. KGaA, Weinheim]. (b) Second-order correlation function graph. The dip at zero-time delay confirms high single photon purity. Reproduced from [115]. CC BY 4.0. (c) Schematic representation of a photonic circuit with the InAsP/InP dot-in-wire playing the role of quantum light emitter. (d) Steps of the fabrication, including the pick of a single nanowire containing the dot, its horizontal deterministic positioning and the subsequent fabrication of the SiN_x waveguide and the rest of the quantum photonic circuit. Reproduced from [117]. CC BY 4.0.

photon sources on-chip and deterministically filter the transitions of a specific individual source. One of the most important tools for filtering in such a configuration is the monochromator. The most fundamental function of a monochromator is the transmission of a narrow range of wavelengths, which is selected from a wider band of emitted light. This can be achieved via dispersion in a prism or via the use of a diffraction grating to separate light of different wavelength ranges. The selected light can then be transmitted towards an avalanche photodiode (APD) for on-chip detection. Apart from the monochromator, an intriguing alternative is the use of ring resonators to achieve filtering. Optical ring resonators are essentially a series of waveguides with one or more of them forming a closed loop. The light that resonates with the latter is increased in intensity via following multiple routes around the closed loop based on the principle of constructive interference. Hence, ring resonators can be used as both amplifiers and filters, since only the selected light that resonates with the setup will build up in intensity.

As part of the scalability of NWQD single photon sources in quantum photonic circuits, on-chip filtering has been a great challenge to accomplish the isolation of the individual quantum states of the single photon source. A crucial step has been achieved via the successful on-chip single photon filtering, using InAsP single QDs in InP NWs encapsulated by the photonic channel [117]. The latter is comprised of a SiN cladding layer with polymethyl methacrylate (PMMA). The circuit consists of a tunable ring resonator acting as a filter of the quantum states via the principles that were analyzed above. The schematics are shown in figure 13(c) [117]. It is important to underline that the NWQD was positioned horizontally, while the waveguide and circuit were fabricated later. This ensured the deterministic positioning of the single photon source. The procedure is depicted in figure 13(d) [117]. A significant feature of this circuit is the tuning of the wavelengths that are filtered by the ring resonator. This can be achieved by altering the voltage. More specifically, higher voltage has the ability to shift the resonating light to lower wavelengths.

It is interesting to observe the different performances of the aforementioned ring resonator setup and the commercial monochromator in terms of on-chip light filtering. For this reason, a circuit including two monochromators, and a correlator was employed and is illustrated in figure 14(a) [117]. The NWQD was excited by a 532 nm green laser and two cases were examined. In case 1, the generated single photon is directed towards a beam splitter and the two resulting beams

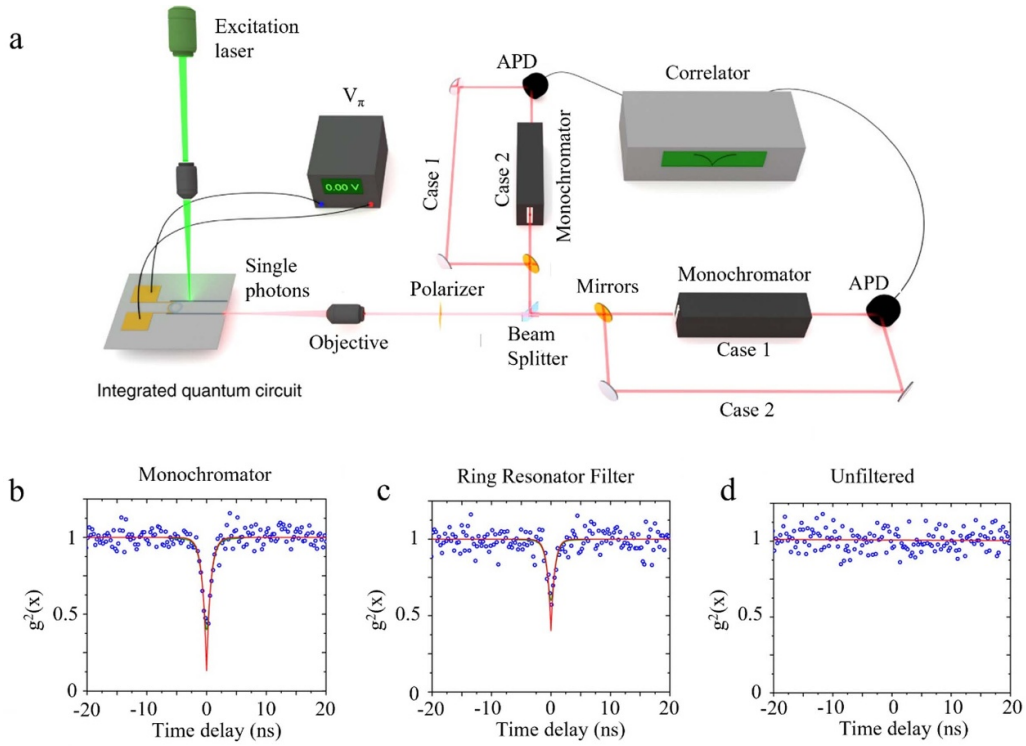

Figure 14. (a) Schematic representation of the setup for the on-chip excitation of the single photon source, using a monochromator as a filter. It is noted that the monochromator can be replaced by a ring resonator filter. (b)–(d) Second-order correlation function at various time delays, for monochromator, ring resonator and unfiltered emission, respectively. The value of the function at zero-time delay is 13%, 40% and 100% for (b)–(d), respectively. Reproduced from [117]. CC BY 4.0.

are guided to two monochromators followed by their detection using two APDs, before eventually being correlated. In case 2, the procedure was the same, but the monochromator branches were circumvented. Hence, the photons were detected by the APDs directly, without prior filtering. Consequently, the three examined scenarios were namely (a) filtering via monochromators, (b) filtering via a ring resonator and (c) emission without filtering. The $g^2(0)$ measurements via the HBT experiment revealed high single photon purity for scenarios a and b, while no quantum light was detected in scenario c. The measurements are presented in figures 14(b)–(d), showing $g^2(0)$ of 13% and 40% for the monochromator and ring resonator, respectively, while no single photon emission was evidenced in the case of unfiltered photons [117]. It is noted that despite the importance of APD as a filter, its non-linear function renders the investigation of other alternatives imperative. Hence, the ring resonator operating at low voltage has been proven a viable and controllable option in terms of on-chip non-classical light emission filtering.

Besides, another challenge has been the multiplexing and demultiplexing of on-chip quantum light deriving from different emitters. This, albeit crucial in the scalability of quantum photonic circuits and the on-chip qubit rate, is demanding in terms of architecture complexity. One solution suggests the use of the tunable ring resonator filter. Two NWQDs are excited separately, leading to the formation of a quantum multiwavelength integrated channel [117]. Initially, the collected spectrum from the through-port of the waveguide is comprised of a multiplexed ensemble of two transitions, spatially separated by 10 nm. This is shown in figure 15(a). Following emission, the photons are decoupled from the main transmission waveguide with the wavelength being the criterion of decoupling. The tunable ring resonator filter is used for the demultiplexing of the emission. Specifically, it couples the resonant optical modes to the drop-port of the photonic circuit, exclusively. This is fully controllable by the filter tuning voltage (V_{π}) that is applied to the ring resonator [117]. The relevant schematic representation is exhibited in figure 15(b). Furthermore, the PL spectra of the QDs vs the applied voltage are presented in figure 15(c), where an increase in V_{π} leads to decoupling of the QD1 peak from the drop-port and correspondingly to coupling of the QD2 peak [117]. The above strongly suggests multiplexing and demultiplexing of entangled photon pairs on-chip.

It is interesting to observe that due to the aforementioned progress, novel platforms in terms of device fabrication have been proposed. A prototypical example is the hybrid SiN/III–V system on a piezoelectric crystal, which facilitates strain tuning [118]. The voltage is tuned between −600 V and 600 V in integrals of 5 V and is applied on the piezoelectric substrate, which generates strain. This strain that is formed on the piezoelectric crystal is then transferred initially to the surface oxide via the deposited layers and eventually reaches the QD embedded in the NW as a result of the NW/oxide van der Waals forces [119]. It is noted that negative voltage leads to compression of the photonic substrate, while positive voltages causes its

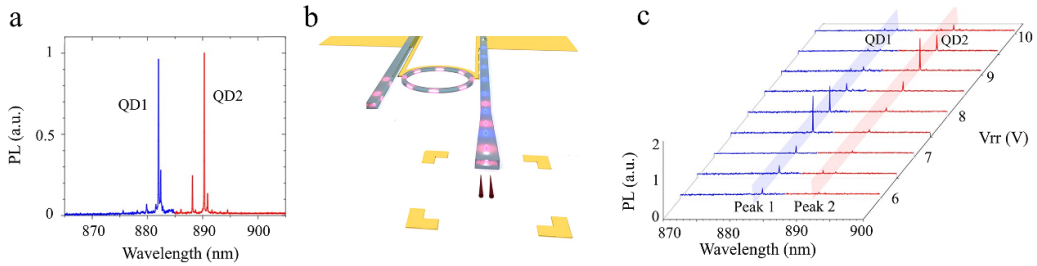

Figure 15. (a) PL spectrum comprised of two individual transitions indicating signal multiplexing. (b) Schematic representation of the demultiplexing function, where the tunable ring resonator couples the resonant optical modes to the drop-port, as a function of the applied voltage (V_{rr}). (c) PL spectra as a function of the V_{rr}. At low voltages, peak 1 at 880 nm is dominant, while increasing voltage leads to the decoupling of peak 1 from the drop-port and the coupling of peak 2, spatially located at 890 nm. Reproduced from [117]. CC BY 4.0.

expansion. After the application of this strain on the InP/InAsP NWQD, the spectra are simultaneously recorded and it can be shown that QD emission is blueshifted (redshifted) for negative (positive) voltages [118]. The relationship between the wavelength and the voltage is linear and the tuning range reaches 39 nm. In addition, an increase in the strain transfer efficiency from the substrate to the NWQD can be achieved by encapsulating the NW with 20 nm of SiN and 200 nm of SiO_x. The tuning range is increased to 1.6 nm, which is more than the quadruple value of the non-encapsulated NWQDs, where the strain transfer was deriving from the van der Waals forces generated at the NW/substrate interface [118]. These suggest a method to achieve a strain-tunable platform with the higher rigidness of the NW/substrate interface and a wider wavelength tuning range.

Despite the importance and the progress in the field of III–V NWQDs, there are important challenges that need to be addressed. Primarily, as mentioned in the review, the interfaces between the NW material (acting as barrier) and the QD (active region) need to be atomically sharp with minimal intermixing. It is interesting to clarify that unavoidable intermixing especially in the case of self-catalyzed NWs has resulted in dot-in-wires not reaching the ultrahigh single photon purity observed in QDs. Nevertheless, the careful optimization of growth parameters such as V/III ratio and temperature have allowed researchers to obtain adequately abrupt interfaces thus achieving low $g^2(0)$ values. Another challenge that arises is the existence of polytypism, as observed by a mixture of ZB and WZ crystal phases in NW structures, which can directly influence the optical properties of the NWQDs, due to alterations in the bandgap energy. Moreover, high density of rotational twins and stacking faults can lead to band bending and carrier scattering jeopardizing the NWQD emission. However, the careful design of the structures such as adequate choice of material combination with minimal strain and the optimization of growth conditions have partially addressed the aforementioned issues with high crystal quality having been obtained.

Apart from the structural aspect of single photon purity from NWQDs, their integration on-chip in quantum photonic circuits has been the topic of extensive scrutiny. Factors that have proven to be challenging are related to the intricacy of the device architecture and the combination of scalability, high efficiency, low cost, and isolation of individual quantum states on the same chip. The results of our review demonstrate the potential and properties of the fabricated quantum photonic circuits in terms of on-chip light generation, voltage-tunable wavelength, filtering and (de)multiplexing, which are major steps towards quantum computing.

6. Discussions and conclusions

6.1. Summary and discussion of the described results

The results that are described in the current review cover the entirety, up to our knowledge, of the existing literature on the rich and vibrant topic of single dot-in-wire structures and their role in single photon generation. As thoroughly discussed in the report, the basic advantage of the formation of the narrower bandgap material, dot-like structure in the NW is the deterministic and controllable positioning, which is challenging in conventional and popular SK growth mode, along with the benefits of the NW geometry. More specifically, these benefits include the inherent waveguide nature of the NW, the lack of threading dislocations, the large strain tolerance and the facilitation of emission collection and coupling with fundamental modes of free space, especially via tapered morphologies [44, 45].

Semiconductors group III–V are an advantageous material platform for the aforementioned structures owing to the high carrier mobility, the optically active nature and the narrow bandgap, while ternary alloys are particularly attractive due to the bandgap tunability, offering an enhanced degree of freedom in the structural design [5]. For those reasons, ternary III–V alloys have been selected as the focus of the current review. In addition, ternary III-nitrides are of equal significance and were included in the report because of their wider bandgap nature and their promising potential for RT operation [94] and electrically driven applications [93]. It is interesting to point out that the acquisition of NWQDs occurs via two main approaches, the top-down fabrication and the bottom-up growth. In the former, the NWs are etched down from as-grown bulk material, which, albeit straightforward, entails a series of disadvantages, such as the additional processing steps, the rough surface and the inclusion of potentially detrimental threading dislocations [39–42]. For these reasons, the majority of the works are focusing on the latter, where the

NWQDs are synthesized epitaxially following the VLS growth mode, where a liquid droplet (either foreign metal or a material of the NWQD) drives the layer-by-layer synthesis of the NWs. The collection of incoming elemental fluxes which dissolve in the liquid droplet leads to supersaturation, which in turn causes the nucleation of a material layer at the liquid/solid interface. The continuation of this procedure signifies the NW elongation [43]. As for the QD, the narrower bandgap material is introduced in ternary NWQDs via the introduction (as is the case in GaAs/InGaAs [25, 82–84]) or cessation (for example in AlGaAs/GaAs [62–67] or GaAsP/GaAs [52, 57, 72]) of the supply of an elemental for a few seconds, allowing for the dot to be formed and embedded axially in the NW.

The results have been interesting in terms of single photon emission deriving from the structures. Each of the platforms employed has shown unique characteristics and advantages but also considerable challenges. In the widely popular AlGaAs/GaAs platform, the benefits include the lack of strain due to the identical lattice constants, the coverage of the important red to near-infrared region of the spectrum and the good barrier properties of AlGaAs, which facilitates carrier confinement in the dot region. For this reason, several works have focused on the synthesis of single GaAs QDs in AlGaAs NWs, with antibunching phenomena being observed [62–67]. Nevertheless, the inhomogeneous nature of Al distribution, which tends to adhere to the bottom sidewall facets due to its low diffusivity, along with the spontaneous formation of an Al-rich AlGaAs shell [72], renders the structure challenging in maintaining high single photon purity as a result of intermixing and less sharp interfaces. In addition, the self-formation of branches further enhances the intricacy of the aforementioned material platform by altering the 1D configuration of NWQDs [75, 76]. Despite these difficulties, there have been promising signs of photon antibunching behavior, albeit marginal at 51% [72].

Another intriguing combination is GaAsP/GaAs, as the wider bandgap of GaAsP renders it a good candidate as a barrier for quantum confinement in the dot region. The results indicate strong exciton and biexciton transitions, with the sharp QD related peak located at 1.66 eV [52]. Even though this peak vanishes at higher temperatures above 60 K, which is a major limitation in industrial applications, the good optical properties and promising potential constitute GaAsP/GaAs an interesting material platform for further investigation. Operation at higher temperatures of 160 K has also been reported in the past. Interestingly, good photon antibunching and strong peaks were sustained up to this temperature, while a high DOP was also measured at 82.5% [21]. This function is crucial for entangled photon pair generation. The main challenge in the case of GaAsP is the direct-to-indirect bandgap transition at high P contents, which limits the window of compositional modifications that can be applied without rendering the structures optically inactive. In addition, P-related growth remains a substantial hazard due to the toxicity of white P, signifying that additional components and precautions should be taken into consideration upon designing the nanostructures.

Apart from binary QDs in ternary NWs, III–V platform can be used vice versa, as is the case for InGaAs QDs embedded in GaAs NWs. The insertion of multiple InGaAs segments on-axis of an GaAs NWs has led to the acquisition of lasers, with a threshold pump of 250 μJ cm^{-2} [82]. Moreover, tailoring of the emission energy of the dot-in-wires can occur via modifications in the size of the InGaAs QD. This has achieved circumvention of inhomogeneous broadening and narrow peaks of 9.3 meV [83]. Among the various accomplishments of this material platform, particular significance has been paid to the realization of a room-temperature operating laser, where 50 InGaAs dots were inserted in GaAs/AlGaAs/GaAs core/shell/-cap [25]. The threshold was low at 25 μJ cm^{-2}, while the transition from broad spontaneous emission to amplified emission is observed at 1.43 eV. The stimulated emission is exhibited even at RT, which is a major step towards NWQD applicability in on-chip devices. Nevertheless, it is interesting to underline, that there are no reports of single photon emission based on InGaAs/GaAs NWQDs, potentially due to intermixing and lack of sharp interfaces that are key for reliable photon antibunching.

A final interesting platform that has been investigated and reported in the frame of the current review is III-nitrides. The wide bandgap of InGaN/GaN or AlGaN/GaN combination along with the thermal stability are excellent features promoting a high level of quantum confinement in dot-in-wire structures, with the carrier leakage being negligible. This signifies that room-temperature functionality can be demonstrated, as lack of carrier escape is crucial for maintaining low $g^2(0)$ even at elevated temperatures, which is a major obstacle in III–V semiconductor materials. Hence, RT single photon sources have been obtained in crystal phase GaN QDs in AlGaN NWs, with a low $g^2(0)$ of 33% even at 300 K [94]. In addition, the strong built-in electric field of III-nitrides enables carrier separation at the two NW ends, which is promising for electrically driven devices. Such steps have been achieved in InGaN/GaN NWQDs, where Mg and Si doping led to p-n junction formation with the dot being the active region. Single photon emission was observed at low temperatures, while highly polarized emission was also noticed, promising for entangled photon pair generation [93].

As established previously in the current review, the most important challenges associated with NWQD single photon emitters are the carrier escape, the shallow interfaces and limitations in terms of electrical injection. Despite the geometrical uniqueness of NWQDs and the exploitation of the NW waveguide effect, the size of the dot which laterally expands in the scale of several nm, inherently poses obstacles in achieving a $g^2(0)$ as low as in the case of conventional QDs. However, it has been shown that crystal phase GaN QDs have maintained an adequately low $g^2(0)$ up to 300 K. This is indicative of the fact that with appropriate and meticulous design of the structures, their architecture and tailored properties, single photon emitters based on NWQDs can be achieved and the advantages of the geometrical features of NWs can be exploited towards on-chip functional devices.

One interesting point is the tailoring of the dot size, which can have a direct influence on the wavelength of the emission. The dependence of the spectral emission to the dimensions of the QD has been well-established, with larger dots emitting at substantially high wavelengths, whereas smaller dots tend to emit towards the low wavelength region of the spectrum. The modulation of the emission energy via modification of the dot size has been demonstrated in NWQDs as well with promising results having been reported. First, the progressively shorter growth duration has led to narrow peaks of 9.3 meV [83], while narrower GaAs QDs in AlGaAs NWs allowed for the GaAs emission to be kept at a particular wavelength regardless of the impact of the Al content in the barrier material [66]. The above exhibits the importance of structural design in the optical response of the NWQDs and show their potential in implementation in various devices including lasers, single photon sources and photodetectors.

6.2. Discussion of our original work

The synthesis of single dots in NWs with the aim to serve as high-quality single photon sources has attracted attention and has been the focal point of investigations in our research group. AlGaAs/GaAs, in particular, has been considered exceptionally vibrant owing to the large strain accommodation and the potential to emit in the important near-infrared region of the spectrum. Ergo, we have focused on synthesizing single GaAs QDs in AlGaAs NWs over the past years, with good results having been reached.

Specifically, bare AlGaAs NWs grown on GaAs stems were first extensively scrutinized. We synthesized AlGaAs NWs with nominal Al contents of 10%, 20%, 30% and 40% [75]. The morphological and structural features of the NWs were closely inspected via SEM and TEM and was observed that frequent variations included kinking, bending and most importantly spontaneous branching. The branching events increased dramatically with Al composition, while compositional analysis allowed us to conclude that the external NW regions are Al-rich [75]. This confirmed the self-formation of an AlGaAs shell, with enhanced surface roughness. The concavities of the shell act as accumulation regions for Ga, due to its higher diffusion length, where the accumulated Ga adatoms nucleate eventually causing the branch elongation [75]. Interestingly, the NWs exhibited a unique feature, where Ga accumulation in the branch itself led to the formation of a checked pattern, with stripes of Ga segregation along and across the branch axial direction intersecting, causing the synthesis of Ga-rich boxes, which is promising for self-assembly of non-classical light emitters [76].

Besides, the NW optical response was also investigated. Fully tunable emission was observed in the red and near-infrared region of the spectrum depending on Al composition. The NWs acted as hosts for the embedding of a single GaAs dot, whose optical properties were also studied [75]. It was found that the dot related emission shows a clear spatially localized nature in the near-infrared region, as anticipated, with strong excitonic and biexcitonic transitions [75]. The linewidth remains low at 490 μeV, strongly suggesting purity of the emission. Furthermore, the NWQDs were based on the self-catalyzed, bottom-up approach, signifying circumvention of Au-associated challenges.

Apart from the aforementioned material platform, works in our group also approached the vibrant yet challenging topic of GaAsP/GaAs single NWQDs, with good results having been reported [53]. Specifically, the structures exhibit good morphological, standing characteristics and uniform morphology. No kinking is observed, which is indicative of the good maintenance of interfacial energetics during the brief cessation of P supply for the dot to be formed [53]. The NWs have no visible defects that could be detrimental to the optical quality of potential devices, while good emission properties are demonstrated, with the GaAs peak showing high level of localization and high brightness, suggestive of good radiative efficiency even at low excitation power. At elevated power of excitation, sharp transitions occur, suggesting charged excitonic or multi-excitonic transitions. This is attributed to strong confinement of the Coulomb-shifted carriers [53]. The limitations that have been analyzed related to temperature and relevant thermal excitation of carriers, which leads to their escape from the confinement region are presented in the current work as well, with the dot-related peak rapidly quenching with increasing temperatures. Eventually, it is worth mentioning that the enhanced optical properties can be partially also ascribed to the formation of a thin passivation shell, which neutralized surface states and circumvented the frequently observed phenomenon of non-radiative recombination following carrier trapping at the highly dense NW surface states [53].

To summarize, in the current report we presented the literature regarding the growth of ternary III–V NWQDs, by initially highlighting their importance in optoelectronic applications followed by the analysis of the growth techniques. Next, we focused on the material platforms that have been used for acquisition of III–V NWQDs divided into two subcategories, namely the ones using GaAs QDs and the ones using ternary QDs, while also referring to the interesting topic of III-N structures. Besides, we underlined the importance of NWQDs towards quantum information processing applications, by including recent works exhibiting high single photon purity. Eventually, we briefly described quantum photonic circuits using NWQDs as single photon sources. Our work encapsulates the progress made on the vibrant topic of ternary III–V NWQDs and their link to quantum information processing and can assist in a comprehensive study of these structures and their future wide-scale implementation in the field of quantum photonics.

Data availability statement

No new data were created or analysed in this study.

Acknowledgments

The authors acknowledge the support of the UK Engineering and Physical Sciences Research Council-EPSRC (Grant Nos. EP/W002302/1) and EPSRC National Epitaxy Facility.

Conflict of interest

The authors declare no competing financial interest.

ORCID iDs

Giorgos Boras https://orcid.org/0000-0002-7760-422X
Huiyun Liu https://orcid.org/0000-0002-7654-8553

References

[1] LaPierre R R, Robson M, Azizur-Rahman K M and Kuyanov P 2017 A review of III–V nanowire infrared photodetectors and sensors *J. Phys. D: Appl. Phys.* **50** 123001
[2] Yan R, Gargas D and Yang P 2009 Nanowire photonics *Nat. Photon.* **3** 569–76
[3] Martensson T, Svensson C P T, Wacaser B A, Larsson M W, Seifert W, Gustafsson A, Wallenberg L R and Samuelson L 2004 Epitaxial III–V nanowires on silicon *Nano Lett.* **4** 1987–90
[4] Tong Q Y and Gösele U 1999 *Semiconductor Wafer Bonding, Science and Technology* (Wiley) pp 204
[5] Boras G, Yu X and Liu H 2019 III–V ternary nanowires on Si substrates: growth, characterisation and device applications *J. Semicond.* **40** 101301
[6] Zhang Y, Aagesen M, Holm J V, Jorgensen H I, Wu J and Liu H 2013 Self-catalyzed GaAsP nanowires grown on silicon substrates by solid-source molecular beam epitaxy *Nano Lett.* **13** 3897–902
[7] Zhang Y, Wu J, Aagesen M, Holm J, Hatch S, Tang M, Huo S and Liu H 2014 Self-catalyzed ternary core-shell GaAsP nanowire arrays grown on patterned Si substrates by molecular beam epitaxy *Nano Lett.* **14** 4542–7
[8] Wu J *et al* 2014 Wafer-scale fabrication of self-catalyzed 1.7 eV GaAsP core-shell nanowire photocathode on silicon substrates *Nano Lett.* **14** 2013–8
[9] Holm J V, Jorgensen H I, Krogstrup P, Nygard J, Liu H and Aagesen M 2013 Surface-passivated GaAsP single-nanowire solar cells exceeding 10% efficiency grown on silicon *Nat. Commun.* **4** 1498
[10] Li L *et al* 2017 Near full-composition-range high-quality $GaAs_{1-x}Sb$ nanowires grown by molecular-beam epitaxy *Nano Lett.* **17** 622–30
[11] Sharma M, Ahmad E, Dev D, Li J, Reynolds C L Jr, Liu Y and Iyer S 2018 Improved performance of GaAsSb/AlGaAs nanowire ensemble Schottky barrier based photodetector via *in situ* annealing *Nanotechnology* **30** 034005
[12] Huh J, Yun H, Kim D-C, Munshi A M, Dheeraj D L, Kauko H, van Helvoort A T J, Lee S, Fimland B-O and Weman H 2015 Rectifying single GaAsSb nanowire devices based on self-induced compositional gradients *Nano Lett.* **15** 3709–15
[13] Yu X, Li L, Wang H, Xiao J, Shen C, Pan D and Zhao J 2016 Two-step fabrication of self-catalyzed Ga-based semiconductor nanowires on Si by molecular-beam epitaxy *Nanoscale* **8** 10615–21
[14] Heiß M, Gustafsson A, Conesa-Boj S, Peiro F, Morante J R, Abstreiter G, Arbiol J, Samuelson L and Fontcuberta I Morral A 2009 Catalyst-free nanowires with axial $In_xGa_{1-x}As$/GaAs heterostructures *Nanotechnology* **20** 075603
[15] Heiß M, Ketterer B, Uccelli E, Morante J R, Arbiol J and Fontcuberta I Morral A 2011 In(Ga)As quantum dot formation on group-III assisted catalyst-free InGaAs nanowires *Nanotechnology* **22** 195601
[16] Unitt D C, Bennett A J, Atkinson P, Cooper K, See P, Gevaux D, Ward M B, Stevenson R M, Ritchie D A and Shields A J 2005 Quantum dots as single-photon sources for quantum information processing *J. Opt. B: Quantum Semiclass. Opt.* B **7** S129
[17] Ren B-C and Deng F-G 2015 Hyper-parallel photonic quantum computation with coupled quantum dots *Sci. Rep.* **4** 4623
[18] Othaman Z, Boo L K, Sakrani S and Muhammad R 2008 The Stranski-Krastanov three dimensional islands growth prediction of finite size model (part I) *J. Fiz. UTM* **3** 78–83
[19] Francaviglia L, Fontana Y and Fontcuberta I Morral A 2016 Quantum Dots in Nanowires *Semiconductors and Semimetals* (Elsevier Inc.) ch 5, pp 94
[20] Mäntynen H, Anttu N, Sun Z and Lipsanen H 2019 Single-photon sources with quantum dots in III–V nanowires *Nanophotonics* **8** 747–69
[21] Yu P *et al* 2019 Nanowire quantum dot surface engineering for high temperature single photon emission *ACS Nano* **13** 13492–500
[22] Makhonin M N, Foster A P, Krysa A B, Fry P W, Davies D G, Grange T, Walther T, Skolnick M S and Wilson L R 2013 Homogeneous array of nanowire-embedded quantum light emitters *Nano Lett.* **13** 861–5
[23] Minot E D, Kelkensberg F, van Kouwen M, van Dam J A, Kouwenhoven L P, Zwiller V, Borgstrom M T, Wunnicke O, Verheijen M A and Bakkers E P A M 2007 Single quantum dot nanowire LEDs *Nano Lett.* **7** 367–71
[24] Versteegh M A M, Reimer M E, Jöns K D, Dalacu D, Poole P J, Gulinatti A, Giudice A and Zwiller V 2014 Observation of strongly entangled photon pairs from a nanowire quantum dot *Nat. Commun.* **5** 5298
[25] Tatebayashi J, Kako S, Ho J, Ota Y, Iwamoto S and Arakawa Y 2015 Room-temperature lasing in a single nanowire with quantum dots *Nat. Photon.* **9** 501–5
[26] Ho J, Tatebayashi J, Sergent S, Fong C F, Ota Y, Iwamoto S and Arakawa Y 2016 A nanowire-based plasmonic quantum dot laser *Nano Lett.* **16** 2845–50
[27] Tatebayashi J, Ota Y, Ishida S, Nishioka M, Iwamoto S and Arakawa Y 2018 Nanowire-quantum-dot lasers on flexible membranes *Appl. Phys. Express* **11** 065002
[28] Goldner P, Ferrier A and Guillot-Noël O 2015 Rare earth-doped crystals for quantum information processing *Handbook on the Physics and Chemistry of Rare Earths* vol 46 (Elsevier Inc.) pp 1–78
[29] Shor P W 1994 Algorithms for quantum computation: discrete logarithms and factoring *Proc. 35th Annual Symp. on Foundations of Computer Science* pp 124–34
[30] Deshpande S, Frost T, Hazari A and Bhattacharya P 2014 Electrically pumped single-photon emission at room temperature from a single InGaN/GaN quantum dot *Appl. Phys. Lett.* **105** 141109
[31] Kako S, Santori C, Hoshino K, Götzinger S, Yamamoto Y and Arakawa Y 2006 A gallium nitride single-photon source operating at 200 K *Nat. Mater.* **5** 887–92
[32] O'Brien J L 2007 Optical quantum computing *Science* **318** 1567–70
[33] Langford N K, Ramelow S, Prevedel R, Munro W J, Milburn G J and Zeilinger A 2011 Efficient quantum

computing using coherent photon conversion *Nature* **478** 360–3
[34] He Y-M, He Y, Wei Y-J, Wu D, Atatüre M, Schneider C, Höfling S, Kamp M, Lu C-Y and Pan J-W 2013 On-demand semiconductor single-photon source with near-unity indistinguishability *Nat. Nanotechnol.* **8** 213–7
[35] Shields A J 2007 Semiconductor quantum light sources *Nat. Photon.* **1** 215–23
[36] Chanana A *et al* 2022 Ultra-low loss quantum photonic circuits integrated with single quantum emitters *Nat. Commun.* **13** 7693
[37] Hepp S, Jetter M, Portalupi S L and Michler P 2019 Semiconductor quantum dots for integrated quantum photonics *Adv. Quantum Technol.* **2** 1900020
[38] Arthur J R 2002 Molecular beam epitaxy *Surf. Sci.* **500** 189–217
[39] Munsch M, Claudon J, Bleuse J, Malik N S, Dupuy E, Gerard J M, Chen Y, Gregersen N and Mork J 2012 Linearly polarized single-mode spontaneous emission in a photonic nanowire *Phys. Rev. Lett.* **108** 077405
[40] Claudon J, Bleuse J, Malik N S, Bazin M, Jaffrenou P, Gregersen N, Sauvan C, Lalanne P and Gerard J M 2010 A highly efficient single-photon source based on a quantum dot in a photonic nanowire *Nat. Photon.* **4** 174–7
[41] Bleuse J, Claudon J, Creasey M, Malik N S, Gerard J M, Maksymov I, Hugonin J P and Lalanne P 2011 Inhibition enhancement and control of spontaneous emission in photonic nanowires *Phys. Rev. Lett.* **106** 103601
[42] Yeo I *et al* 2014 Strain mediated coupling in a quantum dot-mechanical oscillator hybrid system *Nat. Nanotechnol.* **9** 106–10
[43] Dubrovskii V G 2015 Theory of VLS growth of compound semiconductors *Semiconductors and Semimetals* (Elsevier Inc.) ch 1, pp 93
[44] Reimer M E, Bulgarini G, Akopian N, Hocevar M, Bavinck M B, Verheijen M A, Bakkers E P A M, Kouwenhoven L P and Zwiller V 2012 Bright single-photon sources in bottom-up tailored nanowires *Nat. Commun.* **3** 737
[45] Dalacu D, Mnaymneh K, Lapointe J, Wu X, Poole P J, Bulgarini G, Zwiller V and Reimer M E 2012 Ultraclean emission from InAsP quantum dots in defect-free wurtzite InP nanowires *Nano Lett.* **12** 5919–23
[46] Tatebayashi J, Ota Y, Ishida S, Nishioka M, Iwamoto S and Arakawa Y 2012 Site-controlled formation of InAs/GaAs quantum-dot-in-nanowires for single photon emitters *Appl. Phys. Lett.* **100** 263101
[47] Ohlsson B, Bjork M, Persson A, Thelander C, Wallenberg L, Magnusson M, Deppert K and Samuelson L 2002 Growth and characterisation of GaAs and InAs nano-whiskers and InAs/GaAs heterostructures *Physica* E **1386–947713** 1126–30
[48] Bjork M T, Ohlsson B J, Sass T, Persson A I, Thelander C, Magnusson M H, Deppert K, Wallenberg L R and Samuelson L 2002 One dimensional heterostructures in semiconductor nanowhiskers *Appl. Phys. Lett.* **80** 1058–60
[49] Borgstrom M T, Zwiller V, Muller E and Imamoglu A 2005 Optically bright quantum dots in single nanowires *Nano Lett.* **5** 1439–43
[50] Reznik R R, Shtrom I V, Samsonenko Y B, Khrebtov A I, Soshnikov I P and Cirlin G E 2017 The dependence of the wavelength on MBE growth parameters of GaAs quantum dot in AlGaAs NWs on Si(111) substrate *J. Phys.: Conf. Ser.* **929** 012047
[51] Zhang Y, Wu J, Aagesen M and Liu H 2015 III–V nanowires and nanowire optoelectronic devices *J. Phys. D: Appl. Phys.* **48** 463001
[52] Dick K A and Caroff P 2014 Metal-seeded growth of III–V semiconductor nanowires: towards gold-free synthesis *Nanoscale* **6** 3006–21
[53] Wu J *et al* 2016 Defect-free self-catalyzed GaAs/GaAsP nanowire quantum dots grown on Si substrate *Nano Lett.* **16** 504–11
[54] Birowosuto M D, Yokoo A, Zhang G, Tateno K, Kuramochi E, Taniyama H, Takiguchi M and Notomi M 2014 Movable high-Q nanoresonators realized by semiconductor nanowires on a Si photonic crystal platform *Nat. Mater.* **13** 279–85
[55] Persson A I, Bjork M T, Jeppesen S, Wagner J B, Wallenberg L R and Samuelson L 2006 $InAs_{1-x}P_x$ nanowires for device engineering *Nano Lett.* **6** 403–7
[56] Trägårdh J, Persson A I, Wagner J B, Hessman D and Samuelson L 2007 Measurements of the band gap of wurtzite $InAs_{1-x}P_x$ nanowires using photocurrent spectroscopy *J. Appl. Phys.* **101** 123701
[57] Saxena D, Mokkapati S, Parkinson P, Jiang N, Gao Q, Tan H H and Jagadish C 2013 Optically pumped room-temperature GaAs nanowire lasers *Nat. Photon.* **7** 963–8
[58] Tambe M J, Lim S K, Smith M J, Allard L F and Gradecak S 2008 Realization of defect-free epitaxial core/shell GaAs/AlGaAs nanowire heterostrucctures *Appl. Phys. Lett.* **93** 151917
[59] Krogstrup P, Curiotto S, Johnson E, Aagesen M, Nygard J and Chatain D 2011 Impact of liquid phase shape on the structure of III–V nanowires *Phys. Rev. Lett.* **106** 125505
[60] Hoang T B, Titova L V, Yarrison-Rice J M, Jackson H E, Govorov A O, Kim Y, Joyce H J, Tan H H, Jagadish C and Smith L M 2007 Resonant excitation and imaging of nonequilibirum exciton spins in single core-shell GaAs-AlGaAs nanowires *Nano Lett.* **7** 588–95
[61] Titova L V, Hoang T B, Jackson H E, Smith L M, Yarrison-Rice J M, Kim Y, Joyce H J, Tan H H and Jagadish C 2006 Temperature dependence of photoluminescence from single core-shell GaAs-AlGaAs nanowires *Appl. Phys. Lett.* **89** 173126
[62] Koblmüller G, Mayer B, Stettner T, Abstreiter G and Finley J J 2017 GaAs-AlGaAs core-shell nanowire lasers on silicon: invited review *Semicond. Sci. Technol.* **32** 053001
[63] Kats V N, Kohеresko V P, Platonov A V, Chizhova T V, Cirlin G E, Bouravleuv A D, Samsonenko Y B, Soshnikov I P, Ubyivovk E V and Bleuse J 2012 Optical study of GaAs quantum dots embedded into AlGaAs nanowires *Semicond. Sci. Technol.* **27** 015009
[64] Cirlin G E, Reznik R R, Shtrom I V, Khrebtov A I, Samsonenko Y B, Kukushkin S A, Kasama T, Akopian N and Leonard L 2018 Hybrid GaAs/AlGaAs nanowire-quantum dot system for single photon sources *Semiconductors* **52** 462–4
[65] Kochereshko V P, Kats V N, Platonov A V, Cirlin G E, Bouravleuv A D, Samsonenko Y B, Besombes L and Mariette H 2013 GaAs single quantum dot embedded into AlGaAs nanowire *AIP Conf. Proc.* **1566** 482
[66] Platonov A V, Kochereshko V P, Kats V N, Tsyrlin G E, Buravlev A D, Samsonenko Y B, Besombes L and Mariette H 2013 Optical properties of individual GaAs quantum dots embedded into AlGaAs nanowires *J. Synch. Invest.* **7** 622–5
[67] Cirlin G E, Reznik R R, Shtrom I V, Khrebtov A I, Soshnikov I P, Kukushkin S A, Leandro L, Kasama T and Akopian N 2017 AlGaAs and AlGaAs/GaAs/AlGaAs nanowires grown by molecular beam epitaxy on silicon substrates *J. Phys. D: Appl. Phys.* **50** 484003

[68] Leandro L, Gunnarsson C P, Reznik R, Jöns K D, Shtrom I, Khrebtov A, Kasama T, Zwiller V, Cirlin G and Akopian N 2018 Nanowire quantum dots tuned to atomic resonances *Nano Lett.* **18** 7217–21

[69] Tietjen J J and Amick J A 1966 The preparation and properties of vapor-deposited epitaxial $GaAs_{1-x}P_x$ using arsine and phosphine *J. Electrochem. Soc.* **113** 724

[70] Wu Z H, Sun M, Mei X Y and Ruda H E 2004 Growth and photoluminescence characteristics of AlGaAs nanowires *Appl. Phys. Lett.* **85** 657–9

[71] Chen C, Shehata S, Fradin C, LaPierre R, Couteau C and Weihs G 2007 Self-directed growth of AlGaAs core-shell nanowires for visible light applications *Nano Lett.* **7** 2584–9

[72] Dubrovskii V G, Shtrom I V, Reznik R R, Samsonenko Y B, Khrebtov A I, Soshnikov I P, Rouvimov S, Akopian N, Kasama T and Cirlin G E 2016 Origin of spontaneous core-shell AlGaAs nanowires grown by molecular beam epitaxy *Cryst. Growth Des.* **16** 7251–5

[73] Loitsch B, Winnerl J, Grimaldi G, Wierzbowski J, Rudolph D, Morkötter S, Döblinger M, Abstreiter G, Koblmüller G and Finley J J 2015 Crystal phase quantum dots in the ultrathin core of GaAs-AlGaAs core-shell nanowires *Nano Lett.* **15** 7544–51

[74] Dietrich C P, Fiore A, Thompson M G, Kamp M and Höfling S 2016 GaAs integrated quantum photonics: towards compact and multi-functional quantum photonic integrated circuits *Laser Photon. Rev.* **10** 870

[75] Boras G *et al* 2021 Self-catalyzed AlGaAs nanowires and AlGaAs/GaAs nanowire-quantum dots on Si substrates *J. Phys. Chem.* C **125** 14338–47

[76] Boras G, Yu X, Fonseka H A, Zhang D, Zeng H, Sanchez A M and Liu H 2020 Checked patterned elemental distribution in AlGaAs nanowire branches via vapor-liquid-solid growth *Nanoscale* **12** 15711–20

[77] Tchernycheva M, Cirlin G E, Patriarche G, Travers L, Zwiller V, Perinetti U and Harmand J-C 2007 Growth and characterisation of InP nanowires with InAsP insertions *Nano Lett.* **7** 1500–4

[78] Cirlin G E, Tchernycheva M, Patriarche G and Harmand J-C 2012 Effect of postgrowth heat treatment on the structural and optical properties of InP/InAsP/InP nanowires *Semiconductors* **46** 175–8

[79] Chang T-Y, Kim H, Hubbard W A, Azizur-Rahman K M, Jun J J, Kim J-H, Lee W-J and Huffaker D 2022 InAsP quantum-dot embedded inp nanowires toward silicon photonic applications *ACS Appl. Mater. Interfaces* **14** 12488–94

[80] Singh R and Bester G 2009 Nanowire quantum dots as an ideal source of entangled photon pairs *Phys. Rev. Lett.* **103** 063601

[81] Sergienko A and Jaeger G 2003 Quantum information processing and precise optical measurement with entangled-photon pairs *Contemp. Phys.* **44** 341–56

[82] Bourennane M, Eibl M, Gaertner S, Kurtsiefer C, Cabello A and Weinfurter H 2004 Decoherence-free quantum information processing with four-photon entangled states *Phys. Rev. Lett.* **92** 107901

[83] Tatebayashi J, Kako S, Ho J, Ota Y, Iwamoto S and Arakawa Y 2017 Growth of InGaAs/GaAs nanowire-quantum dots on AlGaAs/GaAs distributed Bragg reflectors for laser applications *J. Cryst. Growth* **468** 144–8

[84] Tatebayashi J, Ota Y, Ishida S, Nishioka M, Iwamoto S and Arakawa Y 2014 Highly uniform, multi-stacked InGaAs/GaAs quantum dots embedded in a GaAs nanowire *Appl. Phys. Lett.* **105** 103104

[85] Tatebayashi J, Ota Y, Ishida S, Nishioka M, Iwamoto S and Arakawa Y 2013 Formation and optical properties of multi-stack InGaAs quantum dots embedded in GaAs nanowires by selective metalorganic chemical vapor deposition *J. Cryst. Growth* **370** 299–302

[86] Mokhov E N and Wolfson A A 2019 Growth of AlN and GaN crystals by sublimation *Electronic and Optical Materials, Single Crystals of Electronic Materials* (Woodhead Publishing) pp 401–45

[87] Kane M H and Arefin N 2014 Gallium nitride (GaN) on silicon substrates for LEDs *Nitride Semiconductor Light-Emitting Diodes (Leds)* (Woodhead Publishing) pp 99–143

[88] Fu H and Zhao Y 2018 Efficiency droop in GaInN/GaN LEDs *Electronic and Optical Materials, Nitride Semiconductor Light-Emitting Diodes (Leds)* (Woodhead Publishing) pp 299–325

[89] Arita M, Le Roux F, Holmes M J, Kako S and Arakawa Y 2017 Ultraclean single photon emission from a GaN quantum dot *Nano Lett.* **17** 2902–7

[90] Deshpande S, Frost T, Yan L, Jahangir S, Hazari A, Liu X, Mirecki-Millunchick J, Mi Z and Bhattacharya P 2015 Formation and nature of InGaN quantum dots in GaN nanowires *Nano Lett.* **15** 1647–53

[91] Aiello A, Hoque A K M H, Baten M Z and Bhattacharya P 2019 High-gain silicon-based InGaN/GaN dot-in-nanowire array photodetector *ACS Photonics* **6** 1289–94

[92] Wang Z L *et al* 2017 Manipulating the band bending of InGaN/GaN quantum dots in nanowires by surface passivation *J. Phys. Chem.* C **121** 6380–5

[93] Deshpande S, Heo J, Das A and Bhattacharya P 2013 Electrically driven polarized single-photon emission from an InGaN quantum dot in a GaN nanowire *Nat. Commun.* **4** 1675

[94] Holmes M J, Choi K, Kako S, Arita M and Arakawa Y 2014 Room-temperature triggered single photon emission from a III-nitride site-controlled nanowire quantum dot *Nano Lett.* **14** 982–6

[95] Holmes M J, Kako S, Choi K, Podemski P, Arita M and Arakawa Y 2015 Probing the excitonic states of site-controlled GaN nanowire quantum dots *Nano Lett.* **15** 1047–51

[96] Deshpande S, Das A and Bhattacharya P 2013 Blue single photon emission up to 200 K from an InGaN quantum dot in AlGaN nanowire *Appl. Phys. Lett.* **102** 161114

[97] Barettin D, Platonov A V, Pecchia A, Kats V N, Cirlin G E, Soshnikov I P, Buravleuv A D and Besombes L 2013 Model of GaAs quantum dot embedded in a polymorph AlGaAs nanowire *IEEE J. Sel. Top. Quantum Electron.* **19** 1–9

[98] Marquardt O, Caro M A, Koprucki T, Mathe P and Willatzen M 2020 Multiband k·p model and fitting scheme for *ab initio* based electronic structure parameters for wurtzite GaAs *Phys. Rev.* B **101** 235147

[99] Barettin D, Shtrom I V, Reznik R R, Mikushev S V, Cirlin G E, Auf der Maur M and Akopian N 2023 Direct band gap AlGaAs wurtzite nanowires *Nano Lett.* **23** 895–901

[100] Barettin D, Shtrom I V, Reznik R R and Cirlin G E 2023 Model of a GaAs quantum dot in a direct band gap AlGaAs wurtzite nanowire *Nanomaterials* **13** 1737

[101] Barettin D, Madsen S, Lassen B and Willatzen M 2012 Computational methods for electromechanical fields in self-assembled quantum dots *Commun. Comput. Phys.* **11** 797–830

[102] Barettin D, Lassen B and Willatzen M 2008 Electromechanical fields in GaN/AlN wurtzite quantum dots *J. Phys.: Conf. Ser.* **107** 012001

[103] Grünwald P 2019 Effective second-order correlation function and single-photon detection *New J. Phys.* **21** 093003
[104] Anderson M, Müller T, Skiba-Szymanska J, Krysa A B, Huwer J, Stevenson R M, Heffernan J, Ritchie D A and Shields A J 2021 Coherence in single photon emission from droplet epitaxy and Stranski-Krastanov quantum dots in the telecom C-band *Appl. Phys. Lett.* **118** 014003
[105] Tribu A, Sallen G, Aichele T, Andre R, Poizat J-P, Bougerol C, Tatarenko S and Kheng K 2008 A high-temperature single-photon source from nanowire quantum dots *Nano Lett.* **8** 4326–9
[106] Bounouar S *et al* 2012 Ultrafast room temperature single-photon source from nanowire-quantum dots *Nano Lett.* **12** 2977–81
[107] Stachurski J, Tamariz S, Callsen G, Butte R and Grandjean N 2022 Single photon emission and recombination dynamics in self-assembled GaN/AlN quantum dots *Light Sci. Appl.* **11** 114
[108] Boretti A, Rosa L, Mackie A and Castelletto S 2015 Electrically driven quantum light sources *Adv. Opt. Mater.* **3** 1012–33
[109] Deshpande S and Bhattacharya P 2013 An electrically driven quantum dot-in-nanowire visible single photon source operating up to 150 K *Appl. Phys. Lett.* **103** 241117
[110] Basset F B *et al* 2021 Quantum key distribution with entangled photons generated on demand by a quantum dot *Sci. Adv.* **7** eabe6379
[111] Ilday S *et al* 2016 Multiscale self-assembly of silicon quantum dots into an anisotropic three-dimensional random network *Nano Lett.* **16** 1942–8
[112] Pooley M A, Ellis D J P, Patel R B, Bennett A J, Chan K H A, Farrer I, Ritchie D A and Shields A J 2012 Controlled-NOT gate operating with single photons *Appl. Phys. Lett.* **100** 211103
[113] Zadeh I E, Elshaari A W, Jöns K D, Fognini A, Dalacu D, Poole P J, Reimer M E and Zwiller V 2016 Deterministic integration of single photon sources in silicon based photonic circuits *Nano Lett.* **16** 2289–94
[114] Mnaymneh K, Dalacu D, McKee J, Lapointe J, Haffouz S, Weber J F, Northeast D B, Poole P J, Aers G C and Williams R L 2020 On-chip integration of single photon sources via evanescent coupling of tapered nanowires to SiN waveguides *Adv. Quantum Technol.* **3** 1900021
[115] Laferriere P, Yeung E, Miron I, Northeast D B, Haffouz S, Lapointe J, Korkusinski M, Poole P J, Williams R L and Dalacu D 2022 Unity yield of deterministically positioned quantum dot single photon sources *Sci. Rep.* **12** 6376
[116] Harris N C, Grassani D, Simbula A, Pant M, Galli M, Baehr-Jones T, Hochberg M, Englund D, Bajoni D and Galland C 2014 Integrated source of spectrally filtered correlated photons for large-scale quantum photonic systems *Phys. Rev.* X **4** 041047
[117] Elshaari A W, Zadeh I E, Fognini A, Reimer M E, Dalacu D, Poole P J, Zwiller V and Jöns K D 2017 On-chip single photon filtering and multiplexing in hybrid quantum photonic circuits *Nat. Commun.* **8** 379
[118] Elshaari A W *et al* 2018 Strain-tunable quantum integrated photonics *Nano Lett.* **18** 7969–76
[119] Chen Y *et al* 2016 Controlling the exciton energy of a nanowire quantum dot by strain fields *Appl. Phys. Lett.* **108** 182103